Cosmological constraints on new scalar gravitational interactions

by

Aaron Plahn
B.Sc., Thompson Rivers University, 2012

Thesis Submitted in Partial Fulfillment
of the Requirements for the Degree of

Master of Science

in the
Department of Physics
Faculty of Science

Simon Fraser University
Spring 2015

APPROVAL

Name:	Aaron Plahn
Degree:	Master of Science
Title of Thesis:	Cosmological constraints on new scalar gravitational interactions
Examining Committee:	Dr. Eldon Emberly, Associate Professor, Chair

Dr. Levon Pogosian, Senior Supervisor
Associate Professor, Physics,
SFU

Dr. Andrei Frolov, Supervisor
Associate Professor, Physics,
SFU

Dr. Howard Trottier, Supervisor,
Professor, Physics,
SFU

Dr. Dugan O'Neil, Internal Examiner
Professor, Physics,
SFU

Date Approved: January 9, 2015

Partial Copyright Licence

Abstract

Scalar-Tensor theory is a framework for modified gravity that encompasses many well-studied alternatives to General Relativity. Of particular interests are theories which possess a screening mechanism, which allows for the satisfaction of the bounds of solar system and laboratory scale tests of gravity, while giving rise to novel effects on cosmological scales. Among these are Large-Curvature $f(R)$ as well as Chameleon, Symmetron and Dilaton gravity. All of these models can be described in terms of a recently introduced parametrization of Scalar-Tensor Theory, which involves two free functions of time alone. These models have been implemented by modifying the existing code MGCAMB. In this thesis, we discuss our implementation of these models. We present the results of Fisher forecasts for the constraints on the parameters of the 4 aforementioned models, taking the Large Synoptic Survey Telescope (LSST) and Planck as representative surveys. We also use the Principal Components Analysis approach, forecasting constraints for bins of the two functions upon discretization.

I would like to dedicate this work to the memory of Robert Frazier. Sadly on June 7, 1991 suddenly passed away. Robert Frazier was a kind, fun loving, creative and spirited young man studying in Science at Thomson Rivers University (TRU). I was very fortunate to receive a Fellowship in his name through TRU, where I also studied Science as an undergrad. I hope that his memory lives on through this work.

Acknowledgments

First I'd like to thank my wife Jolene and daughter Briseis for their support and patience along the way. I am grateful for the excellent supervision I received from Dr. Levon Pogosian. He has encouraged my progress while being patient and understanding. I am greatly indebted to Dr. Alireza Hojjati for all of the technical assistance he has given me along the way. He has unbelievable passion for Cosmology, and as busy as he is with the great research he does, he always makes time to help others. I was fortunate to have the opportunities to serve as Teacher's Assistant to Dr. Howard Trottier and Dr. Andrew Debenedictis, both of whom share my passion for teaching and outreach. I also want to thank Dr. Andrei Frolov, both for serving on my committee and for always sharing his seemingly endless knowledge about Physics, Mathematics and Computer Programming among other subjects. I'd like to thank Shao-Jie Yin, Jun-Qi Guo, Yang Liu, Cheng Tang, Yun Li, Micah Brush and Joshua Aftergood for making the Cosmology group at SFU fun to be part of, and wish them the best of luck in the future. I am grateful to the Physics office staff for always making things run seamlessly. Finally, I thank the Graduate Physics Caucus for their hard work.

Contents

List of Tables

List of Figures

Chapter 1

The Standard Model of Cosmology

1.1 General Relativity

1.1.1 Foundations and Observations

General Relativity (GR) is at current our most successful theory of gravity, theoretically as well as empirically. GR describes gravity in purely geometric terms. It attributes gravitation to the geometry of spacetime. The dynamical field is the metric, a rank 2 tensor. The field equations are second order in the metric derivatives.

The classical tests of GR include precession of the orbit of Mercury, lunar ranging and gravitational lensing of light by the sun. The latter was the subject of the famous Eddington expedition which first confirmed the deflection angle predicted by GR, which differs by a factor of 2 from the Newtonian result. Today the deflection angle is measured to be that expected from GR within one part in 10^4 [1]. Time delay experiments involving radio links with space craft have confirmed the gravitational time delay expected due to GR within one part in 10^5 [2]. Both of these tests are probes of null geodesics.

The anomalous precession of the perihelion of Mercury probes spacelike geodesics. In relativistic theories of gravity, in contrast with the Newtonian theory, the orbits of a test particle about an isolated mass fail to close, causing the perihelion to precess. GR predicts a precession of $\Delta\omega = 42.98''$ for Mercury [3]. The current best bound is $\Delta\omega = 42.984 \pm .061$ [4].

1.1.2 The Einstein Field Equations

For completeness, the essentials of GR are reviewed here [5, 6]. The Riemann tensor is central to describing the geometry of a (pseudo-) Riemannian manifold. It is defined in terms of the metric

and its derivatives to second order as

$$R^{\rho}{}_{\sigma\mu\nu} \equiv \partial_\mu \Gamma^{\rho}_{\nu\sigma} - \partial_\nu \Gamma^{\rho}_{\mu\sigma} + \Gamma^{\rho}_{\mu\lambda}\Gamma^{\lambda}_{\nu\sigma} - \Gamma^{\rho}_{\nu\lambda}\Gamma^{\lambda}_{\mu\sigma}, \tag{1.1}$$

where $\Gamma^{\sigma}_{\mu\nu}$ is the metric connection [1]

$$\Gamma^{\sigma}_{\mu\nu} = \frac{1}{2} g^{\sigma\rho}(\partial_\mu g_{\nu\rho} + \partial_\nu g_{\rho\mu} - \partial_\rho g_{\mu\nu}). \tag{1.2}$$

In (1.1), as throughout, we employ the Einstein summation convention; repeated Greek indices (one covariant and one contravariant) are summed from 0 to 3, while Latin indices are summed from 1 to 3. The former correspond to the (Minkowski) tangent space to the full spacetime, while the latter correspond to the tangent space to a spacelike hypersurface.

A (simply-connected) spacetime is flat iff the Riemann tensor vanishes identically, in which case there exists some coordinate system in which the metric is Minkowski

$$[g_{\mu\nu}] = [\eta_{\mu\nu}] = diag(-1, 1, 1, 1). \tag{1.3}$$

The rank two Ricci tensor is defined from Riemann as

$$R_{\mu\nu} \equiv R^{\gamma}{}_{\mu\gamma\nu}. \tag{1.4}$$

Further contracting yields the Ricci scalar

$$R \equiv R^{\mu}{}_{\mu}. \tag{1.5}$$

The Riemann tensor has $n^2(n^2-1)/12$ independent components in n dimensions. [2]

The Riemann tensor satisfies the Bianchi identity

$$\nabla_{[\lambda} R_{\rho\sigma]\mu\nu} = 0, \tag{1.6}$$

where the brackets denote anti-symmetrization with respect to the enclosed indices. The (twice-) contracted version of this identity is

$$\nabla^{\mu}[R_{\mu\nu} - \frac{1}{2} R g_{\mu\nu}] = 0. \tag{1.7}$$

This identity provides one route to Einstein's field equations. If we choose to describe matter in terms of the energy-momentum tensor $T_{\mu\nu}$, and we want the latter to be conserved $\nabla^{\mu} T_{\mu\nu} \equiv 0$, then the left hand side of (1.7) is the right rank-2 tensor to equate to $T_{\mu\nu}$. The bracketed term in (1.7) is known as the Einstein Tensor. We could add a constant times the metric, whose covariant derivative and hence covariant divergence vanishes identically as a result of metric compatibility of

[1] I.e. it is the unique metric compatible, torsion-free connection.

[2] In 3 dimensions, this coincides with the degrees of freedom in the Ricci tensor, hence the historical importance of $R_{\mu\nu}$.

the covariant derivative defined by the Christoffel connection. Hence the Einstein equations with a Cosmological constant are

$$R_{\mu\nu} - \frac{1}{2}g_{\mu\nu}R + \Lambda g_{\mu\nu} = 8\pi G T_{\mu\nu}, \tag{1.8}$$

where we have set c = 1, as we will continue to do.

An alternate path to the field equations is as follows. The simplest scalar that can be constructed from the metric and its derivatives to second order is the Ricci scalar plus a constant scalar [3]. Hence the simplest Lagrangian second order in the metric is the Hilbert-Einstein Lagrangian with a "cosmological constant" term [4],

$$\mathcal{L} = \frac{\sqrt{-g}}{16\pi G}[R - 2\Lambda]. \tag{1.9}$$

The field equations follow via the principle of least action. Varying (1.9) with respect to the metric yields

$$R_{\mu\nu} - \frac{1}{2}g_{\mu\nu}R + \Lambda g_{\mu\nu} = 0. \tag{1.10}$$

The right hand side of (1.8) following from including the matter action, and defining [5]

$$T_{\mu\nu} \equiv -\frac{1}{\sqrt{-g}}\frac{\delta S_M}{\delta g^{\mu\nu}}. \tag{1.11}$$

.

The cosmological constant term was initially added by Einstein to allow for the possibility of a static solution. However, this solution is instable. Hence the constant term was not considered for a great time. Recent evidence for the accelerated expansion of the universe lead to the resurrection of the cosmological constant, which is now included in the standard model of Cosmology, Λ-Cold Dark Matter (LCDM).

1.2 LCDM

1.2.1 The FRW Universe: Background Evolution

GR allowed for the mathematical study of the universe at a level not before possible. Taking the Copernican principle, we suppose that the universe is very nearly (spatially) homogeneous and isotropic. While initially this seems like a bold postulate, it is recapitulated by the statistics of the Cosmic Microwave Background (CMB). This radiation surrounds us, coming from all directions on the sky. It has a nearly perfect blackbody spectrum, and amazingly the Temperature corresponding to this spectrum is the same from all points on the sky to 1 part in 10^5 [7].

[3] I will be loose with notation in referring to tensor fields simply as tensors, and Lagrangian densities simply as Lagrangians.

[4] One can add additional terms involving contractions of products of Riemann and Ricci with themselves and still obtain second order field equations. However, these terms do not add a contribution to the resulting Euler-Lagrange equations[3].

Mathematically, a spatially homogeneous and isotropic spacetime can be realized as the foliation of maximally symmetric spacelike 3-manifolds. The maximally symmetric 3-manifolds come in three varieties: spherical, flat and hyperbolic. In any of these cases the metric can be put in the form corresponding to the line element

$$ds^2 = -dt^2 + a^2(t)[\frac{dr^2}{1-\kappa r^2} + r^2 d\Omega^2], \tag{1.12}$$

where $a(t)$ is known as the scale factor, whose evolution is to be determined from the Einstein equations, while

$$\kappa = \begin{cases} < 0 & \text{for an open universe} \\ = 0 & \text{for a flat universe} \\ > 0 & \text{for a closed universe} \end{cases}$$

corresponding to hyperbolic, Euclidean and spherical spatial geometry respectively.

Our universe is very close to flat; current observational constraints give $\Omega_\kappa = 0.04 \pm 0.06$, where $\Omega_\kappa = 0$ corresponds to a flat universe [8]. Here we consider the case of a flat spacetime, which is assumed in our numerical work as well. In this case, the Einstein equations (1.8) become

$$(\frac{\dot{a}}{a})^2 = \frac{8\pi G}{3} G a^2 \bar{\rho} \tag{1.13}$$

$$\frac{d}{d\tau}(\frac{\dot{a}}{a}) = -\frac{4\pi}{3} G a^2 (\bar{\rho} + 3\bar{P}), \tag{1.14}$$

where dots denote derivatives with respect to conformal time, and the overbars have been added to ρ and P in anticipation of the inclusion of perturbations.

Clearly, space is not homogeneous and isotropic on the scales that we experience here on Earth. However, on large enough scales the universe is, as a matter of fact, very close to spatial homogeneity and isotropy. Hence cosmologists often study the perturbed FRW universe. There is then a limit to the scales within which this is valid. To study cosmology on smaller scales requires full N-body simulations, which are computationally demanding. We restrict our attention to linear cosmological perturbations.

1.2.2 Gauge Transformations

The field equations are invariant under general change of coordinates. General coordinate covariance leaves us with gauge freedom, which amounts to the freedom to choose a frame with respect to which perturbations are to be defined. Two commonly used gauges are the Conformal Newtonian and Synchronous gauges. Here we shall develop the theory in the Conformal Newtonian gauge, and introduce the relations required to transform to the Synchronous gauge, which is used in CAMB.

In general, perturbations to the metric can be decomposed into scalar, vector and tensor modes with respect to 3-diffeomorphisms on the spatial slices [9]. At the level of linear perturbation theory, these modes are decoupled. Further, it is scalar modes that couple to density fluctuations, and hence the scalar modes are the central focus in the study of structure formation. In what follows, we shall consider only scalar perturbations to the metric.

The Synchronous gauge can be defined by the line element

$$ds^2 = a^2(\tau)[-d\tau^2 + (\delta_{ij} + h_{ij})dx^i dx^j]. \tag{1.15}$$

We will later move to Fourier space. Hence we write the scalar component of h_{ij} as

$$h_{ij}(\vec{x},\tau) = \int d^3k e^{i\vec{k}\cdot\vec{x}}[\hat{k}_i\hat{k}_j h(\vec{k},\tau) + (\hat{k}_i\hat{k}_j - \frac{1}{3}\delta_{ij})6\eta(\vec{k},\tau)], \tag{1.16}$$

where $\hat{k}$ is the unit vector in the direction of $\vec{k}$. There is still residual gauge freedom after this definition, which is absorbed by choosing the frame in which the velocity of CDM vanishes.

The Newtonian gauge is defined by [5]

$$g_{\mu\nu}dx^\mu dx^\nu = a^2(\tau)[-(1+2\Psi)d\tau^2 + (1-2\Phi)dx_i dx^i], \tag{1.17}$$

where Ψ and Φ are scalar perturbations to the metric. By definition, only scalar perturbations to the metric exist in the Newtonian gauge. So while this gauge is not completely general, it is suited to our work.

One can transform between the Synchronous and Newtonian gauges using the following relations [10]

$$\Psi = \frac{1}{2k^2}[\ddot{h} + 6\ddot{\eta} + \frac{\dot{a}}{a}(\dot{h} + 6\dot{\eta})] \tag{1.18}$$

$$\Phi = \eta - \frac{1}{2k^2}\frac{\dot{a}}{a}(\dot{h} + 6\dot{\eta}). \tag{1.19}$$

1.2.3 The Perturbed Einstein Equations

In addition to the metric, the energy-momentum tensor also includes perturbations, which we will denote as follows [10].

$$T_{\mu\nu} = \bar{T}_{\mu\nu} + \delta T_{\mu\nu} \tag{1.20}$$

Meanwhile,

$$\rho = \bar{\rho} + \delta\rho \tag{1.21}$$

$$P = \bar{P} + \delta P. \tag{1.22}$$

[5] Different sign conventions for Φ are common. We follow the convention of [10]

We shall find it convenient to work in Fourier space, following the convention that

$$\Phi(\vec{x},\tau) \equiv \int d^3k d^{i\vec{k}\cdot\vec{x}}\Phi(\vec{k},\tau), \tag{1.23}$$

where we denote the Fourier transform of a function by the same symbol as the function itself, which shall not cause any confusion as we work solely in k-space.

If we define the variables

$$(\bar{\rho}+\bar{P})\theta \equiv ik^j\delta T^0{}_j \tag{1.24}$$

$$(\bar{\rho}+\bar{p})\sigma = -(\hat{k}_i\hat{k}^j - \frac{1}{3}\delta_i{}^j)(T^i{}_j - \frac{T^k{}_k}{3}\delta_i{}^j), \tag{1.25}$$

we can write the perturbed Einstein equations as

$$k^2\Phi + 3\frac{\dot{a}}{a}(\dot{\Phi}+\frac{\dot{a}}{a}\Psi) = 4\pi G a^2\delta T^0{}_0, \tag{1.26}$$

$$k^2(\dot{\Phi}+\frac{\dot{a}}{a}\Psi) = 4\pi G a^2(\bar{\rho}+\bar{P})\theta, \tag{1.27}$$

$$\ddot{\Phi}+\frac{\dot{a}}{a}(\dot{\Psi}+2\dot{\Phi})+2\frac{\ddot{a}}{a}-(\frac{\dot{a}}{a})^2)\Psi+\frac{k^2}{3}(\Phi-\Psi) = \frac{4\pi G}{3}a^2(\bar{\rho}+\bar{P})\delta T^i{}_i \tag{1.28}$$

$$k^2(\Phi-\Psi) = 12\pi G a^2(\bar{\rho}+\bar{P})\sigma. \tag{1.29}$$

It should be noted that the variables introduced in (1.24) and (1.25) are gauge dependent. The relationship between their values in the Newtonian and Synchronous gauges is as follows.

$$\delta^{(SYN)} = \delta^{(CON)} - \alpha\frac{\dot{\bar{\rho}}}{\bar{\rho}} \tag{1.30}$$

$$\theta^{(SYN)} = \theta^{(CON)} - \alpha k^2 \tag{1.31}$$

$$\delta P^{(SYN)} = \delta P^{(CON)} - \alpha\bar{P} \tag{1.32}$$

$$\alpha = \frac{\dot{h}+6\dot{\eta}}{2k^2} \tag{1.33}$$

For later reference, we shall define the matter power spectrum as follows.

$$<\delta(\vec{k})\delta(\vec{k'})> = (2\pi)^3P(k)\delta^3(\vec{k}-\vec{k'}), \tag{1.34}$$

where the angular brackets denote an average over the distribution.

1.2.4 The Boltzmann Equation

We are interested in the statistics of the large scale universe. Hence, we describe the various species of matter in terms of their distributions. While the Einstein equations tell us how matter influences gravity, we also need to know how matter will move in response to gravity. If we are only considering matter as a perfect fluid, then the continuity equation suffices. However, in general we need to include the full distribution functions and non-gravitational interactions [9, 10].

One can describe the (6-dimensional) phase space using the canonically conjugate variables x^i, P_j, where P_j is related to the proper momentum, p_j, measured by an observed with fixed spatial coordinates by

$$P_j = a(1-\Phi)p_j. \tag{1.35}$$

Let f denote the phase space distribution of a given particle species, satisfying

$$f(x^i, P_j, \tau)dx^1dx^2dx^3dP_1dP_2dP_3 = dN, \tag{1.36}$$

where dN is the differential number of particles in a differential 6-volume element of phase space. In the 0th order universe, all species are in equilibrium, and hence we obtain the zero order distributions f_0 given by

$$f_0(\epsilon) = \frac{g_s}{h^3}\frac{1}{e^{\epsilon/(k_bT_0)} \pm 1}, \tag{1.37}$$

where $+$ corresponds to fermions and $-$ to bosons, h is Planck's constant, and k_b is the Boltzmann constant. The energy-momentum tensor of a species is related to its distribution function via

$$T_{\mu\nu} = \int \sqrt{-g}dP_1dP_2dP_3\frac{P_\mu P_\nu}{P^0}f(x^i, P_j, \tau). \tag{1.38}$$

We will work with q and n_j, where $q_j = ap_j$ and $q_j = qn_j$, $\hat{n}$ being a unit vector. We will proceed by writing $f(x^i, P_j, \tau) = f_0[1 - Y(x^i, q, n_j, \tau)]$ and working to first order in Y. The Boltzmann equation is in general

$$\frac{\partial f_i}{\partial \tau} + \frac{dx^i}{d\tau}\frac{\partial f_i}{\partial x^i} + \frac{dq}{d\tau}\frac{\partial f_i}{\partial q} + \frac{dn_i}{d\tau}\frac{\partial f_i}{\partial n_i} = C[f_j], \tag{1.39}$$

where we have added a Latin subscript to the distribution function to track the various species. The collision term on the right hand side is a functional of the distributions for all species. They account for changes in the distribution function brought about by non-gravitational interactions and are obtained by integrating appropriate cross sections calculated using Quantum Field theory over all possible momenta.

From the geodesic equation it follows that

$$\frac{dq}{d\tau} = q\dot{\Phi} - \epsilon(q,\tau)n_i\partial_i\Psi. \tag{1.40}$$

Hence to first order in perturbations (of the metric and distribution functions), the Boltzmann equation in k-space becomes

$$\frac{dY}{d\tau} + i\frac{q}{\epsilon}(\vec{k}\cdot\hat{n})Y + \frac{dlnf_0}{dlnq}[\dot{\Phi} - i\frac{\epsilon}{q}(\vec{k}\cdot\hat{n})]Y = \frac{1}{f_0}(\frac{df}{d\tau})_C. \tag{1.41}$$

One consequence of the Boltzmann equation is that an axially symmetric distribution remains axially symmetric for collisionless particles. Hence axially asymmetric perturbations for collisionless particles do not couple to other species or the metric. For massless collisionless particles, we have $\epsilon = q$, so that we can integrate out the q-dependence in the distribution, defining

$$F(\vec{k}, \eta, \tau) \equiv \frac{\int dq q^3 f_0(q) \Psi}{\int dq q^3 f_0(q)}. \tag{1.42}$$

Since the angular dependence enters only through $\hat{k} \cdot \hat{n}$, we can expand F in a Legendre series:

$$F(\vec{k}, \eta, \tau) \equiv \sum_{l=0}^{\infty} (-i)^l (2l+1) F_l(\vec{k}, \tau) P_l(\hat{k} \cdot \hat{n}), \tag{1.43}$$

where P_l is the l^{th} Legendre polynomial and F_l are the corresponding Legendre components of F. Taking (collisionless) massless neutrinos as an example, one obtains in the Newtonian gauge

$$\dot{\delta}_\nu = -\frac{4}{3}\theta_\nu + 4\dot{\Phi} \tag{1.44}$$

$$\dot{\theta}_\nu = k^2(\frac{1}{4}\delta_\nu - \sigma_\nu) + k^2\Psi \tag{1.45}$$

$$\dot{F}_{\nu l} = \frac{k}{2l+1}[l F_{\nu(l-1)} - (l+1) F_{\nu(l+1)}], l \geq 2. \tag{1.46}$$

Hence we obtain an infinite hierarchy of equations. In practice there are schemes to truncate this hierarchy and maintain the required numerical precision.

In the case of massive particles, we choose instead to expand the perturbation Y directly in a Legendre series:

$$Y(\vec{k}, \hat{n}, q, \tau) \equiv \sum_{l=0}^{l=\infty} (-i)^l (2l+1) Y_l(\vec{k}, \tau) P_l(\hat{k} \cdot \hat{n}). \tag{1.47}$$

Taking massive neutrinos as an example, we have

$$\dot{Y}_0 = -\frac{qk}{\epsilon} Y_1 - \dot{\Phi} \frac{dln f_0}{dln q} \tag{1.48}$$

$$\dot{Y}_1 = \frac{qk}{3\epsilon}(Y_0 - 2Y_2) - \frac{\epsilon k}{3q}\Psi \frac{dln f_0}{dln q} \tag{1.49}$$

$$\dot{Y}_l = \frac{qk}{(2l+1)\epsilon}[l Y_{l-1} - (l+1) Y_{l+1}], l \geq 2. \tag{1.50}$$

In the case of massive particles, the obligatory q dependence in the Boltzmann equation makes the equations computationally more demanding.

Chapter 2

Modified Gravity

2.1 The Dark Energy Problem

The current best-fit model of the universe is LCDM with $\Omega_B \approx 0.05, \Omega_C \approx 0.25$,and$\Omega_\Lambda \approx 0.7$ [3]. In particular, evidence from type Ia supernovae luminosity distances, CMB anisotropies, galaxy clustering among others all support the presence of a component with a negative equation-of-state, $w \equiv P/\rho \approx -1$. What is the nature of this strange substance? If it is truly a cosmological constant, then one may be content to interpret it as a property of the vacuum. However, this leads to problems.

One is the fine-tuning problem. If we attribute the cosmological constant to the vacuum energy that is expected from Quantum Field Theory, one expects a cosmological constant that differs from the observed one by 120 orders of magnitude! One can appeal to unknown physics at the Planck scale. However, this is feigning ignorance. This is the domain of Quantum Gravity, for which 100 years of research have failed to produce a satisfying theory.

Another problem is the so called coincidence-problem. The energy density in matter and that in the cosmological constant are of the same order of magnitude today. Since the energy density in matter scales as a^{-3}, and that in the cosmological constant remain constant, it seems an unlikely coincidence that they should happen to be of the same order now.

Dark Matter too is problematic. There is not yet a compelling candidate for Dark Matter that fits within the Standard Model of Particle Physics. And while there are many theoretically motivated possibilities within popular extensions of the Standard Model, there is not yet compelling evidence for these candidates. Further, the structure of CDM halos as predicted by N body simulations is inconsistent with observations of galaxy density profiles. N-body simulations predict the density profile of CDM to have a cusp and be of the form $\rho \sim 1/r$ or $\rho \sim r^{-\alpha}$ with α close to 1 [11]. Yet galactic cores are observed to flatten out near the center [3]. While it is possible to invent models of DM to alleviate these problems, at current these are speculative at best. Suffice it to say the nature

of Dark Matter is still poorly understood.

An alternative is that a dynamical field is responsible for the accelerated expansion of the universe. Scalar-tensor theories contain a scalar gravitational field, and allow for novel behavior on cosmological scales, which may circumvent the need for exotic components in the energy budget of the universe.

2.2 Scalar-Tensor Theory

Lovelock's theorem states that the only possible second-order Euler-Lagrange expression obtainable in a four dimensional space from a scalar density of the form $\mathcal{L} = \mathcal{L}(g_{\mu\nu})$ is

$$E^{\mu\nu} = \alpha\sqrt{-g}[R^{\mu\nu} - \frac{1}{2}g^{\mu\nu}R + \lambda\sqrt{-g}g^{\mu\nu}], \tag{2.1}$$

where α and λ are constants, and $R^{\mu\nu}$ and R are the Ricci tensor and scalar curvature, respectively [3].

To modify gravity, then, we must relax some of the postulates of Lovelock's theorem. Some possibilities include using higher order field equations, considering extra dimensions and considering a non-symmetric 2nd rank tensor (adding torsion). Another possibility, and the one that we shall pursue, is to add additional fields beyond the metric.

Scalar-tensor theories are constructed by including a gravitational scalar field in addition to the rank-2 metric tensor. We will refer to these theories collectively as "Scalar-Tensor Theory" (STT). The general form of the Lagrangian for STT is [1]

$$\mathcal{L} = \frac{\sqrt{-g}}{16\pi}[\phi R - \frac{\omega(\phi)}{\phi}\nabla_\mu\phi\nabla^\mu\phi - 2\Lambda(\phi)] + \mathcal{L}_m(\Psi_M, g_{\mu\nu}), \tag{2.2}$$

where ω and Λ are arbitrary functions of ϕ, and Ψ_M are some matter fields. The field equations follow from the principle of least action. Varying the action with respect to the metric yields

$$\phi G_{\mu\nu} + [\Box\phi + \frac{1}{2}\frac{\omega}{\phi} + \nabla_\mu\phi\nabla^\mu\phi + \Lambda]g_{\mu\nu} - \nabla_\mu\nabla_\nu\phi - \frac{\omega}{\phi}\nabla_\mu\phi\nabla_\nu\phi = 8\pi T_{\mu\nu}. \tag{2.3}$$

Varying the action with respect to ϕ, and using the trace of metric equation to eliminate R, one obtains the second field equation

$$(2\omega + 3)\Box\phi + \omega'\nabla_\mu\phi\nabla^\mu\phi + 4\Lambda - 2\phi\Lambda' = 8\pi T. \tag{2.4}$$

STT is conformally equivalent to GR- i.e. the field equations can be reduced to those of GR via a conformal transformation of the metric

$$g_{\mu\nu} \to e^{-\Sigma(x^\mu)}g_{\mu\nu} = \bar{g_{\mu\nu}}, \tag{2.5}$$

[1] Technically this form assumes that we are working in the Jordan-frame in which matter is minimally coupled to the additional scalar degree of freedom.

upon which

$$\mathcal{L} \to -\frac{\sqrt{\bar{g}}}{16\pi}\phi e^{2\Sigma}(\bar{R} - 6g^{\mu\nu}\Sigma_{,\mu}\Sigma,\nu - 6\Box\Sigma). \tag{2.6}$$

Choosing $e^{2\Sigma} = \phi^{-1}$ while defining

$$\sqrt{\frac{4\pi}{3+2\omega}} \equiv \frac{\partial\Sigma}{\partial\psi} \tag{2.7}$$

and $8\pi V(\psi) \equiv e^{4\Sigma}\Lambda$, we have [2]

$$\mathcal{L} \to \frac{\sqrt{-\bar{g}}}{16\pi}\bar{R} - \sqrt{-\bar{g}}(\frac{1}{2}\bar{\nabla}_\mu\psi\bar{\nabla}^\mu\psi + V(\psi)) + \mathcal{L}_M(\Psi_M, e^{2\Sigma}g_{\bar{\mu}\nu}). \tag{2.8}$$

The field equations become

$$\bar{R}_{\mu\nu} - \frac{1}{2}\bar{g}_{\mu\nu}\bar{R} = 8\pi[\bar{T}_{\mu\nu} + \bar{\nabla}_\mu\psi\bar{\nabla}_\nu\psi - (\frac{1}{2}\bar{\nabla}_\alpha\psi\bar{\nabla}^\alpha\psi + V)\bar{g}_{\mu\nu}], and \tag{2.9}$$

$$\Box\psi - \frac{dV}{d\psi} = -\sqrt{4\pi}\alpha\bar{T}, \tag{2.10}$$

where

$$\alpha \equiv \frac{1}{\sqrt{3+2\omega}}. \tag{2.11}$$

While (2.9) is formally equivalent to GR with a scalar field ψ in a potential $V(\psi)$, there is an important distinction to be made. From (2.10) it follows that

$$\bar{\nabla}_\mu\bar{T}^{\mu\nu} = \sqrt{4\pi}\alpha\bar{T}\bar{\nabla}^\nu\psi, \tag{2.12}$$

and hence does not vanish in general. Matter no longer falls along geodesics of the metric in the new conformal frame, which is known as the Einstein frame. This is in contrast with the previous frame, known as the Jordan frame, in which matter is minimally coupled to the scalar field, falling along geodesics of the Jordan frame metric. The trade off is that in the Jordan frame the Field equations are mathematically and computationally more complicated. We shall elect to work in the Einstein frame, which allows us to modify existing code to perform calculations.

2.3 The $\{m(a), \beta(a)\}$ parametrization

The action (2.2) contains two free functions of $\phi(x^\mu)$, which by composition are functions of all space and time. Under certain conditions, however, one can reduce the freedom to two functions of time alone. This is one of the benefits of a parametrization recently introduced by [12, 13]. Another is that these functions can be understood intuitively as the mass of the additional scalar field and the strength of its coupling to matter.

[2] Note that hidden in $\mathcal{L}_M is a factor of \sqrt{-g}$, i.e. matter couples to the JF metric.

Recall that the Einstein frame action is

$$S = \int d^4x\sqrt{-\bar{g}}[\frac{\bar{R}}{16\pi G} - \frac{1}{2}\bar{\nabla}_\mu\psi\bar{\nabla}^\mu\psi - V(\psi)] + \int d^4x\sqrt{-g}\mathcal{L}_M(\Psi_M, g_{\mu\nu}), \tag{2.13}$$

where $g_{\mu\nu}$ and $\bar{g}_{\mu\nu}$ denote the Jordan and Einstein frame metrics respectively. If we define the function $A(\psi)$ as

$$A^2(\psi) = e^{\Sigma(\psi)}, \tag{2.14}$$

and

$$\beta(\psi) \equiv m_{pl}\frac{dlnA}{d\psi}, \tag{2.15}$$

we have for the scalar field equation

$$\Box\psi = -\beta T + \frac{dV}{d\psi}, \tag{2.16}$$

which is the usual Klein-Gordon equation with the effective potential

$$V_{eff}(\psi) = V(\psi) - [A(\psi) - 1]T. \tag{2.17}$$

If we are considering pressureless matter, then $T = \rho_M$. This detail is crucial. It has the consequence that the minimum of the effective potential is a function of ρ_M, and hence the effective mass of the scalar field is environmentally dependent.

$$m^2 = \frac{d^2V_{eff}}{d\psi^2}|_{\psi_{min}}. \tag{2.18}$$

This allows for the screening of modified gravity effects in dense environments, which is required to satisfy solar system and lab-based tests of gravity.

To get the physics of Big Bang Nucleosynthesis (BBN) correct, it is required that the scalar field ψ settle to the minimum of its effective potential prior to BBN. If this is not the case, the variation in the particle masses due to the coupling of the scalar field to matter would be sufficient to cause noticeable differences to the relative particle abundances we observe today. If the field has been at this minimum since BBN, and also $m^2 >> H^2$, it follows that knowledge of β and m as functions of the scale factor a are sufficient to reconstruct the dynamics of the theory.

To see this, we start by noting that under our assumptions, at the minimum

$$\frac{dV}{d\psi}|_{\psi_{min}} = -\frac{\beta A\rho_M}{m_{pl}}. \tag{2.19}$$

The time evolution of the field at the minimum of the effective potential is given by

$$\frac{d\psi}{dt} = \frac{3H}{m^2}\beta A\frac{\rho_M}{m_{pl}}. \tag{2.20}$$

In order to ensure that that the time variation of fermion masses is not too great, it must be that $A(\psi) \approx 1$. Using this fact and integrating (2.20), we obtain

$$\psi(a) = \frac{3}{m_{pl}}\int_{a_{ini}}^{a}\frac{\beta(a)}{am^2(a)}\rho_M(a)da + \psi_c, \tag{2.21}$$

where ψ_c is the value of the field at some initial time before BBN. Hence we can write

$$V = V_0 - \frac{3}{m_{pl}^2}\int_{a_{ini}}^{a} \frac{\beta^2(a)}{am^2(a)}\rho_M^2(a)da. \tag{2.22}$$

This allows us to reconstruct the potential given the two functions $m(a)$ and $\beta(a)$, restricting our attention to two functions of time alone. One can choose to study these functions in their full generality to study screened modified gravity models in general, or choose specific functional forms for these functions motivated by existing models. We will use both approaches. In what follows, we introduce several well-studied screened modified gravity models that can be accommodated within the $\{m(a), \beta(a)\}$ parametrization. We note that in our work it is sometimes more convenient to deal with

$$\xi(a) \equiv \frac{H_0}{m(a)}, \tag{2.23}$$

in place of $m(a)$.

2.3.1 Screened Modified Gravity

As mentioned above, a mechanism is required in order for STT to satisfy existing solar system and laboratory based tests of gravity, and yet give rise to novel behavior on cosmological scales. Several screening mechanisms have been proposed corresponding to different modified gravity models. We will consider Large-Curvature f(R), Dilaton, Symmetron, and Chameleon theories of gravity, all of which can be accommodated within the $\{m(a), \beta(a)\}$ parametrization.

In the $\{m(a), \beta(a)\}$ parametrization it is apparent that GR is recovered in the cases that

$$m \to \infty \tag{2.24}$$

or

$$\beta \to 0. \tag{2.25}$$

Hence if some dynamical mechanism exists that causes either of these conditions to be satisfied within the environments common on Earth and the sun (i.e. dense environments), it may be possible to satisfy solar system or laboratory tests. The Chameleon mechanism involves the suppression of the scalar field in dense environments, where its mass becomes very heavy and the corresponding range of the force negligibly small. We will consider Large-Curvature f(R) as well as Generalized Chameleon models, both of which are of this type.

Another possibility is a screening mechanism of the Damour-Polyakov type. This involves an environmentally dependent coupling which tends to zero in dense environments. We will consider Dilaton and Symmetron gravity, both of which involve this type of screening mechanism.

Under the assumption that the effective potential has a matter-dependent minimum, along with a couple of mathematical assumptions satisfied by all of these models, independent of which of these

models we consider, there exists a general screening criterion

$$|\psi_\infty - \psi_c| << 2\beta(\psi_\infty) m_{PL} \Phi_N, \tag{2.26}$$

where ψ_C is the value of the field inside a celestial body, ψ_∞ the value of the field outside the body and Φ_N is the Newtonian potential due to the body. This result comes from comparing the ratio of fifth-force to gravity F_ϕ/F_G in the two regimes $\phi_\infty >> \beta_\infty m_{PL}\Phi_N$ and $\rho_c \to \infty$, where ρ_c is the density of the body. In the former, Newtonian gravity is recovered formally. For this to happen as well in the latter case Equation 2.26 must hold.

In the following subsections, we briefly introduce each of the aforementioned models in terms of the $\{m(a), \beta(a)\}$ parametrization. We also introduce preliminary results of our collaborator Dr. Alireza Hojjati who is using the code to obtain constraints on these models from existing data [16]. He uses a combination of currently available SNe, CMB and BAO data to derive joint constraints on the MG and cosmological parameters, using our MGCAMB code in tandem with CosmoMC [17] to sample the parameter space and the likelihood.

Generalized Chameleon

Chameleon Gravity was introduced in [18]. It is a designer approach to modified gravity. One chooses the potential not from a priori theoretical motivations, but rather to obtain the desired screening of modifications in dense environments. In this theory, the mass of the scalar field is exponentially suppressed in dense environments. What is required is a monotonically decreasing runaway potential and a coupling of matter to the scalar field that is also monotonic in ψ [3]. What is important is that this mechanism allows for order unity couplings. We will consider generalized Chameleon models [12], corresponding to power laws for $m(a)$ and $\beta(a)$.

$$m(a) = m_0 a^{-r} \tag{2.27}$$

$$\beta(a) = \beta_0 a^{-s} \tag{2.28}$$

Preliminary results of Monte Carlo likelihood sampling by [16] are shown in Figures 2.1 and 2.2. Two cases are considered : $r = 3; s = 0$ and $r = s = 0$. The former corresponds to a Generalized Chameleon model, while the latter coincides with the fiducial model for the binned model forecast (for results see Chapter 5). These results aid in choosing fiducial values for $\xi_0 \equiv H_0/m_0$.

In Figure 2.1 it is evident that ξ_0 is more tightly constrained in the case where there is no time-dependence in $m(a)$ and $\beta(a)$ (r = s = 0). Allowing for time dependence in the mass leads to a

[3] In general, each matter species could be allowed to have a distinct coupling to the ψ. We won't consider this generalization here.

likelihood which is not sharply peaked near its maximum and has a broader tail. Hence there is a much broader range of acceptable ξ_0 once we allow for time dependence.

Figure 2.2 shows the 1σ and 2σ contours for Ω_M and ξ_0. Note that the red curves close, although this is not shown explicitly. The range of ξ_0 contained within the 1σ contours provide an indication of the standard deviation on ξ_0 from existing data. The shading, which represents the likelihood itself, is immaterial; only the contours themselves are of interest in this figure.

Large-Curvature f(R)

General $f(R)$ models [20] are described by the action

$$S = \int d^4x\sqrt{-g}\frac{f(R)}{16\pi G}, \tag{2.29}$$

where $f(R)$ is an arbitrary function of the Ricci scalar. $f(R)$ corresponds to a constant value of $\beta(a) = 1/\sqrt{6}$. This generalizes the GR action by replacing the Ricci scalar R with a function thereof. We will restrict our attention to the case in which $f(R)$ can be expanded as

$$f(R) = \Lambda + R - \frac{f_{R_0}}{n}\frac{R_0^{n+1}}{R^n}, \tag{2.30}$$

where Λ is a cosmological constant and R_0 denotes the curvature today, which is a specific $f(R)$ model. These models correspond to

$$m(a) = m_0(\frac{4\Omega_{\Lambda 0} + \Omega_{M0}a^{-3}}{4\Omega_{\Lambda 0} + \Omega_{M0}})^{(n+2)/2}, \tag{2.31}$$

where

$$m_0 = H_0\sqrt{\frac{4\Omega_{\Lambda 0} + \Omega_{M0}}{(n+1)f_{R_0}}}. \tag{2.32}$$

Preliminary results of [16] for f(R) gravity are shown in Figure 2.3. This Figure shows the 1σ and 2σ contours for Ω_M and f_{R0} for $n = 0, 1$ and 2. The range of f_{R0} falling within the 1σ contours gives us a standard deviation for f_{R0} from existing data.

Symmetron

In Symmetron gravity [21], the vacuum expectation value (VEV) of the gravitational scalar field is tuned by the ambient density. Meanwhile, the coupling of the scalar to matter is proportional to the VEV so that in dense environments their coupling tends to zero, shutting off the effects of modified gravity. Symmetron models correspond to

$$m(a) = m_*\sqrt{1 - (a_*/a)^3}, \tag{2.33}$$

$$\beta(a) = \begin{cases} \beta_*\sqrt{1 - (\frac{a_*}{a})^3} & a > a_* \\ = 0 & a \leq a_* \end{cases}$$

Preliminary results of [16] for Symmetron gravity are shown in Figure 2.4. This figure shows the 1σ contours for $1/m_0$ ($= \xi_0/H_0$) and β_0. The ranges of these parameters contained within the contour give standard deviations on these parameters from existing data.

Dilaton

The Dilaton field arises in the low-energy limit of string/M-theory in the strong-coupling regime [22]. Dilaton gravity also exhibits a Damour-Polykov type screening mechanism. This model can be parametrized by

$$\beta(a) = \beta_0 exp[-9A_2 m_{pl}^3 \Omega_{M0} H_0^2 \int_a^1 \frac{da}{m^2(a)a^4}] \tag{2.34}$$

and

$$m^2(a) = 3A_2 H^2(a). \tag{2.35}$$

Preliminary results of [16] for Dilaton gravity are shown in Figure 2.5. This figure shows $1/m_0$-Ω_M contours for the Dilaton model using existing data. We see that ξ_0 ($= H_0/m_0$) is weakly constrained by the data of the present.

In this thesis, we shall offer forecasts for constraints on model parameters from upcoming surveys for the Generalized Chameleon and binned models [4]. See Chapter (5) for these results and discussion.

[4] Forecasts for the other models are in progress.

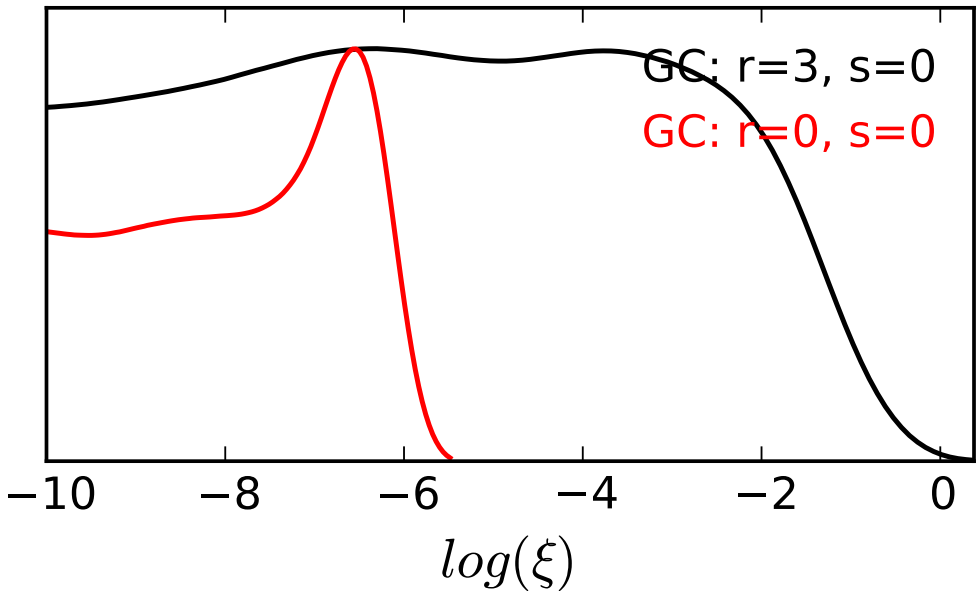

Figure 2.1: Parameter space likelihood for two families of Generalized Chameleon models, corresponding to fixed r and s [16].

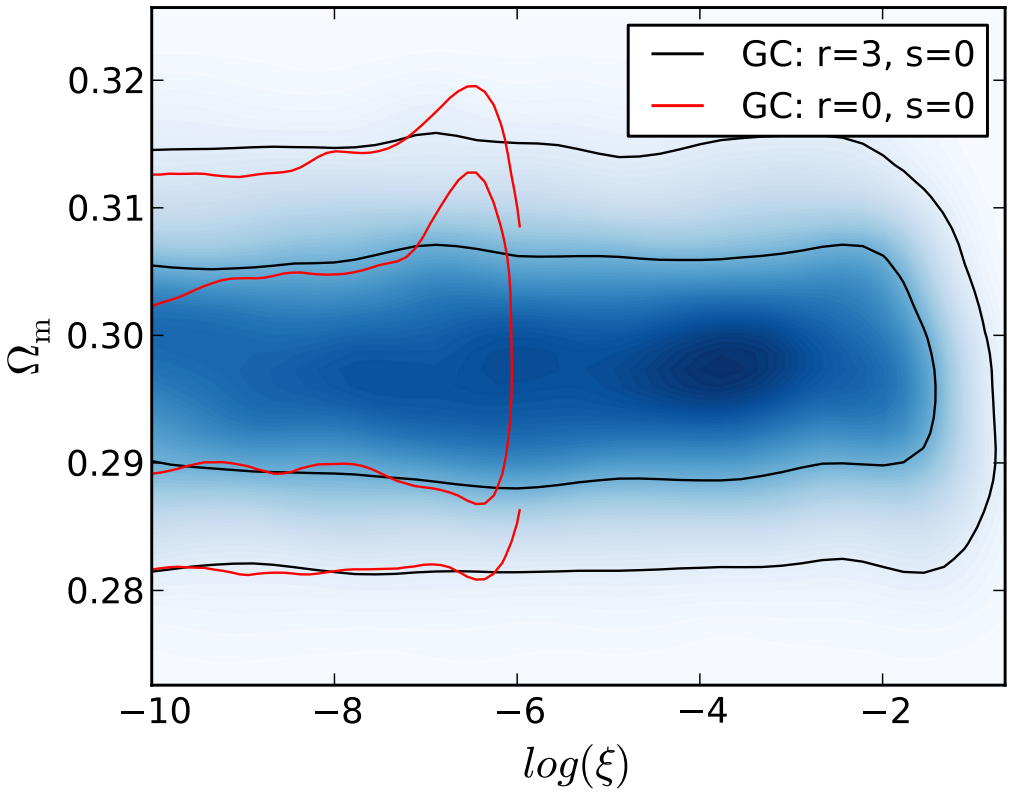

Figure 2.2: Ω_M-ξ_0 contours for two families of Generalized Chameleon models, corresponding to fixed r and s [16].

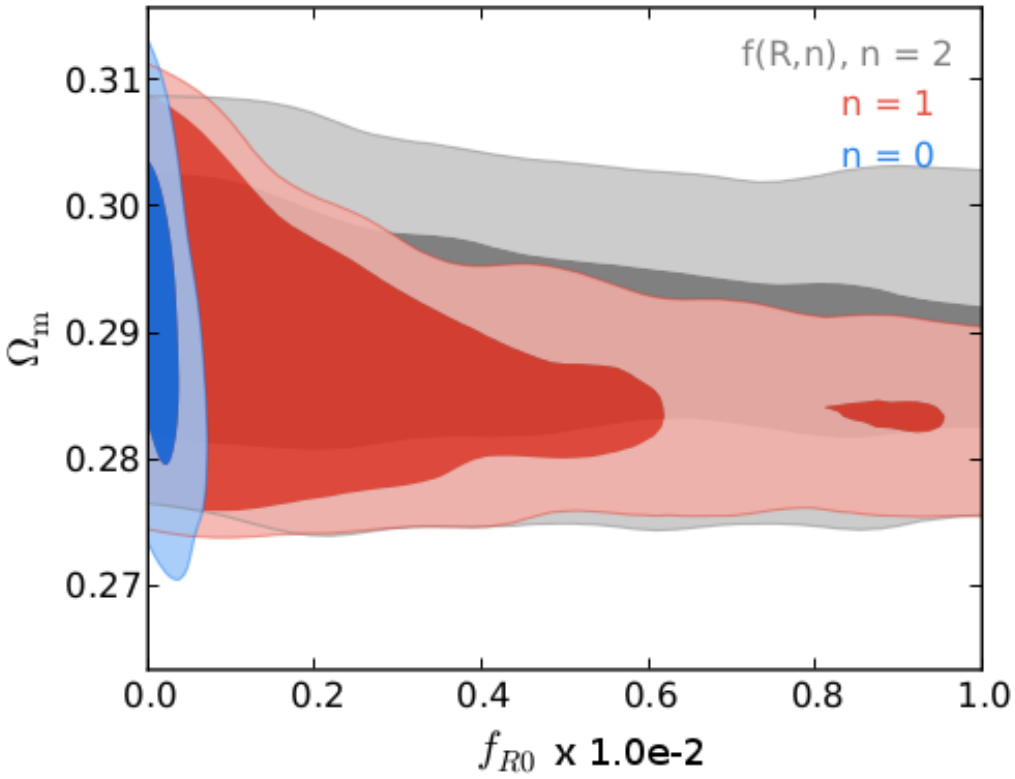

Figure 2.3: Ω_M-f_{R0} contours for three Large-Curvature f(R) models, corresponding to $n = 0, 1$ and 2 [16].

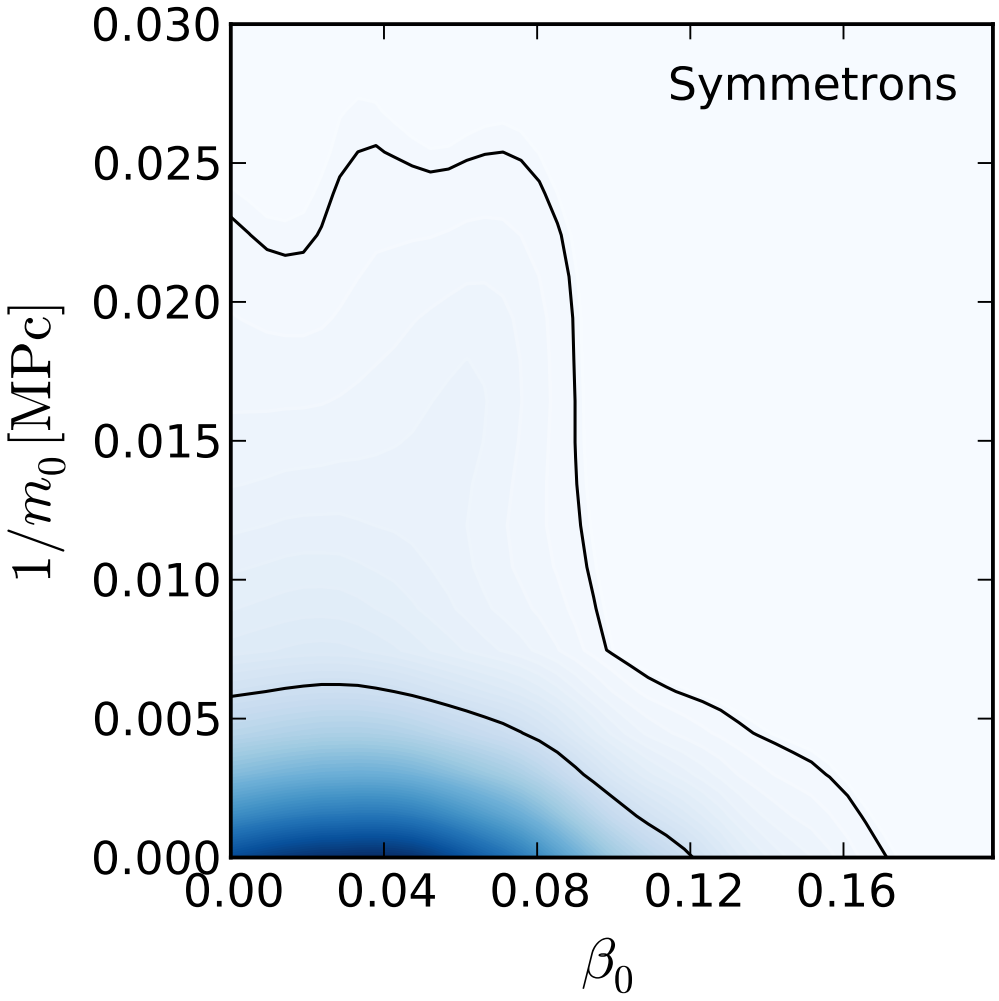

Figure 2.4: $1/m_0$-β_0 contours for the Symmetron model [16].

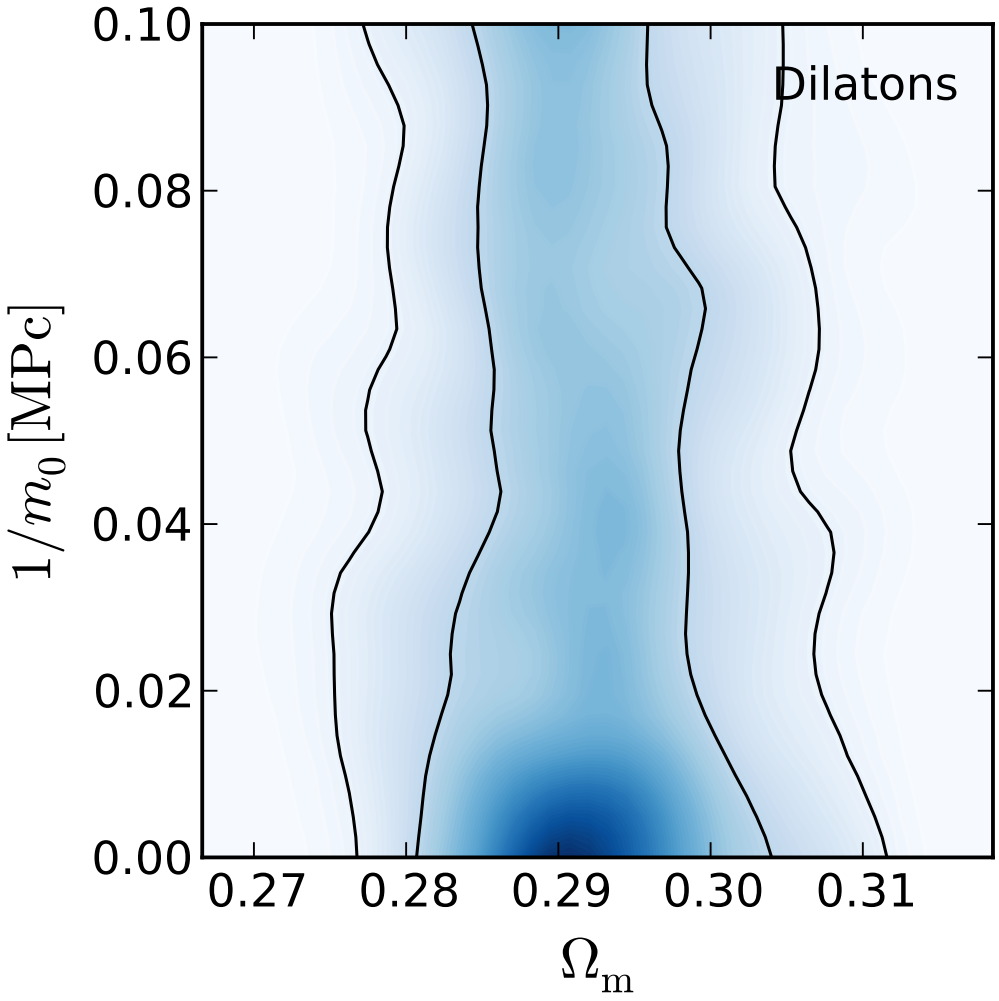

Figure 2.5: $1/m_0$-Ω_M contours for the Dilaton model [16].

Chapter 3

Analysis: Fisher Forecasts and Principal Components Analysis

3.1 Angular Correlations

In LCDM, matter fields are initially drawn from random fields whose statistics are determined by the model of inflation. Hence one can only predict the statistics of the universe, for which we have only one realization.

It is customary to work with angular correlations of observables[15], $C^{ij}(\theta)$, where $\cos(\theta) \equiv \hat{n_1} \cdot \hat{n_2}$, and $\hat{n_1}$ and $\hat{n_2}$ are two directions on the sky. We perform a Legendre expansion of these correlations:

$$C^{ij}(\theta) = \sum_{l=0}^{l=\infty} \frac{2l+1}{4\pi} C_l^{ij} P_l(cos\theta). \tag{3.1}$$

Our observables are CMB temperature and polarization, galaxy counts (GC) and weak lensing shear (WL). GC and WL are measured in N_{GC} and N_{WL} redshift bins, respectively. We consider auto-correlations and cross-correlations of these observables, leading to $\frac{N(N+1)}{2}$ observables in principle, where $N = 2+N_{GC}+N_{WL}$. However, our code does not provide us with cross-correlations of CMB polarization with observables other than CMB temperature. Hence the actual number of types of C_l's we use is

$$3^{\{T\times T+E\times ET\times E\}} + (N_{GC}+N_{WL})^{\{T\times GC/WL\}} + \frac{N_{GC}(N_{GC}+1)}{2}^{\{GC\times GC\}} \tag{3.2}$$

$$+\frac{N_{WL}(N_{WL}+1)}{2}^{\{WL\times WL\}} + N_{GC}N_{WL}^{\{GC\times WL\}}. \tag{3.3}$$

With $N_{GC} = 10$ and $N_{WL} = 6$ we obtain 155 distinct types of C_l's.

3.2 The Fisher Matrix

For our analysis, we make use of the Fisher matrix technique [23] for forecasting the errors to be expected from a joint determination of cosmological and model parameters for several modified gravity models discussed in (Chapter 2). For the binned model, we also make use of the technique of Principal Components Analysis (PCA). Here we briefly review these techniques.

Suppose we have model parameters θ_i for $i = 1, ..., m$, and data x_i for $i = 1, ..., n$. Let $L(\vec{\theta}; \vec{x})$ be the probability distribution function for the parameters given the data. For a fixed set of data, this is the "Likelihood function". We will consider the Fisher matrix, defined as

$$F_{ij} \equiv < \frac{\partial \mathcal{L}}{\partial \theta_i \partial \theta_j} >, \tag{3.4}$$

where $\mathcal{L} \equiv -lnL$. Let $\vec{\theta}_{ML}$ be the estimator of the parameters that maximizes the likelihood. A best unbiased estimator (BUE) is unbiased in that $< \vec{\theta} >= \vec{\theta}_0$, the true value of the parameters, and also minimizes the variances $\Delta\theta_i$. There are theorems that state that if there is a BUE, it is a function of the maximum likelihood estimator, and that the maximum likelihood estimator is in the large-data limit the BUE [23]. A result known as the Cramer-Rao inequality states that

$$\Delta\theta_i \geq \sqrt{F_{ii}^{-1}}, \tag{3.5}$$

which becomes an equality in the large-data limit. Thus the Fisher matrix gives us a lower limit on the parameter errors.

Assuming the likelihood is Gaussian in $\vec{x}$, we obtain

$$F_{ij} = \frac{1}{2} Tr[A_i A_j + C^{-1} M_{ij}], \tag{3.6}$$

where

$$A_i \equiv C^{-1} C_{,i}, \tag{3.7}$$

and

$$M_{ij} \equiv \vec{\mu}_{,i} \vec{\mu}_{,j}^T + \vec{\mu}_{,j} \vec{\mu}_{,i}^T, \tag{3.8}$$

where $\vec{\mu}$ is the mean vector, C the covariance

$$C = < (\vec{x} - \vec{\mu})(\vec{x} - \vec{\mu})^T >, \tag{3.9}$$

and $, i$ denotes partial differentiation with respect to the i^{th} parameter, θ_i. .

In our case, the observables are angular correlations $C_l^{(ij)}$, where i,j label the observables, and the Fisher Matrix is given by [15]

$$F_{ab} = \sum_{l=l_{min}}^{l=l_{max}} (2l+1) \sum_{I=1}^{N} \sum_{J=1}^{N} \frac{\partial \tilde{C_l^I}}{\partial p_a} [\tilde{C_l^{SUB}}^{-1}]_{IJ} \frac{\partial \tilde{C_l^J}}{\partial p_b}, \tag{3.10}$$

where I corresponds to fields $\{i, j\}$ and J to $\{m, n\}$, while

$$[C_l^{\tilde{SUB}}]_{IJ} \equiv C_l^{\tilde{im}} C_l^{\tilde{jn}} + C_l^{\tilde{in}} C_l^{\tilde{jm}}, \tag{3.11}$$

and N is the number of distinct pairs of fields. That is, all pairs of fields are summed over in (3.10). The $C_l^{\tilde{ij}}$ are defined as

$$C_l^{\tilde{ij}} = C_l^{ij} + N_l^{ij}. \tag{3.12}$$

We assume Poisson noise for galaxy counts and weak lensing [15]:

$$N_l^{\kappa_i \kappa_j} = \delta_{ij} \frac{\gamma_{rms}}{n_j} \tag{3.13}$$

$$N_l^{G_i G_j} = \delta_{ij} \gamma_{rms} \frac{1}{n_j} \tag{3.14}$$

$$N_l^{\kappa_i G_j} = 0, \tag{3.15}$$

where γ_{rms} is the expected root mean square shear of the galaxies, and n_j is the number of galaxies per steradian in the j^{th} redshift bin, and G_i and κ_j denote the i^{th} galaxy count and j^{th} weak lensing bin respectively.

For CMB temperature (T) and E-mode polarization (E), the noise is given by

$$Nl^{YY} = [\sum_c (N_{l,c}^{YY})^{-1}]^{-1}, \tag{3.16}$$

with

$$N_{l,c}^{YY} = \frac{\sigma_c^Y \theta_{FWHM,c}}{T_{CMB}} exp[\frac{l(l+1)\theta_{FWHM,c}^2}{8ln2}], \tag{3.17}$$

where Y refers to T or E, c labels the frequency channels for the CMB experiment, $\theta_{FWHM,c}$ is the full-width at half-max of the beam, and in (3.17) we have assumed a Gaussian beam.

For WL and GC we take the Large Synoptic Survey Telescope (LSST) as a representative survey [24], with parameters taken from [25]. For CMB we assume Planck [26], using the three lowest Planck HFI channels, with parameters given in [27].

3.3 Principal Components Analysis

Theories such as Scalar-Tensor theory are typically parametrized by free functions appearing in the action. There are two common courses of action. One can assume a specific functional form for these functions, reducing the freedom to a finite set of parameters. In this case, one must single out a specific model. To study the entire family of models in a more general way, one needs to find a way to study the free functions, which contain in principle infinitely many degrees of freedom.

The data, however, can only constrain certain features of these free functions. Our approach is to discretize these functions using smoothed step functions.

Consider a function $f(a)$ of the scale factor $a = a(\tau)$. Suppose we have defined $f(a)$ discretely in N bins by specifying $m(a_i)$ for $i = 1, ..., N$. Typically, the data is not sufficient to offer strong constraints on the bins of a function, but rather constrains some linear combinations of these bins well. Principal Components Analysis (PCA), which amounts to diagonalizing the Fisher matrix, is a technique that allows one to determine which combinations of the bins will be well constrained.

Suppose that we have calculated the Fisher matrix for the parameters $\{m(a_i), \beta(a_i)\}$ described above [28]. Further, suppose that we have diagonalized this via the following transformation

$$F = W^T \Lambda W, \tag{3.18}$$

where F is the Fisher matrix, Λ is F in the diagonal basis, and W is referred to as the "decorrelation matrix" in this context. Then in the new basis, whose basis vectors with respect to the old basis are given by the columns of W, the parameters are uncorrelated. The diagonal elements $\Lambda_{ii} \equiv \lambda_i$ are related to the errors on these new parameters, which are linear combinations of the physical parameters, via

$$\sigma_i = {\lambda_i}^{-\frac{1}{2}}. \tag{3.19}$$

These eigenvalues can be ordered from the best- to worst- constrained models. We refer to these as the Principal Components (PC's). Typically only the first few PC's will be well-constrained by the observables.

Chapter 4

Numerical Implementation in MGCamb

4.1 CAMB

Code for Anisotropies in the Microwave Background (CAMB) has become the industry standard for numerically evolving Cosmological perturbations from the early universe to today [29]. The user provides cosmological parameters and CAMB integrates the Einstein-Boltzmann equations, producing C_l^{TT},C_l^{TE} and C_l^{EE}. One can also obtain the matter power spectrum and transfer functions. There is also an alternate stream of CAMB, CAMB Sources. CAMB Sources can calculate C_l's for the cross-correlations of weak lensing and galaxy counts in redshift bins. The additional observables make CAMB Sources desirable for performing forecasts.

4.2 MGCAMB

The default version of CAMB assumes GR. It has been modified to incorporate modifications to GR using the $\{\mu(a,k),\gamma(a,k)\}$ parametrization (see 4.2.1). There are two versions of MGCAMB, corresponding to the two versions of default CAMB. MGCAMB V1 [30] is based upon CAMB Sources, and used to generate data for Fisher forecasts. MGCAMB V2 [31] is based upon CAMB and is used together with CosmoMC [17] to obtain fits of model parameters to existing data.

MGCAMB V1 allows the user to choose step sizes for each default and model parameter in addition to the fiducial values supplied. If there are N parameters in total, one run of MGCAMB results in $2N+1$ sets of 158 (1 l and 157 distinct correlations of observables) C_l's corresponding to $2N+1$ sets of parameters p_i. Each parameter is perturbed in turn, once by adding the step

$p \to p + \delta p$ and once by subtracting the step $p \to p - \delta p$. One run using the fiducial values- i.e. leaving all parameters unperturbed- also takes place. This allows for the calculation of derivatives of C_l's with respect to parameters via finite difference.

The $\{m(a), \beta(a)\}$ parametrization is facilitated by the expressions (4.3,4.4) which give $\mu(m(a), \beta(a))$ and $\gamma(m(a), \beta(a))$. MGCAMB requires μ, γ as well as their derivatives with respect to conformal time, which are obtained by implicitly differentiating the (4.3,4.4) expressions with respect to conformal time. For the models considered, the derivatives are computed analytically and used in MGCAMB.

4.2.1 The $\{\mu, \gamma\}$ parametrization

MGCAMB implements modifications to GR within the $\{\mu, \gamma\}$ parametrization [14, 15]. This phenomenological parametrization describes modified gravity in terms of the effective modifications to the Poisson equation and the anisotropy equation, introducing $\mu(k, a)$ and $\gamma(k, a)$ as follows.

$$k^2\Psi = -4\pi G a^2 \mu(k, a)\rho\Delta \tag{4.1}$$

$$\frac{\Phi}{\Psi} = \gamma(k, a). \tag{4.2}$$

In the quasi-static limit, the $\{m(a), \beta(a)\}$ parametrization can be related to the μ, γ parametrization outlined in (Section 2.3). One obtains [12]

$$\mu(k, a) = \frac{(1 + 2\beta^2)k^2 + m^2a^2}{k^2 + m^2a^2} \tag{4.3}$$

$$\gamma(k, a) = \frac{(1 - 2\beta^2)k^2 + m^2a^2}{(1 + 2\beta^2)k^2 + m^2a^2}. \tag{4.4}$$

Expressions (4.3) and (4.4) allow the implementation of STT in the $\{m(a), \beta(a)\}$ parametrization within MGCAMB.

4.3 Finite Differences

Given the C_l data from one run of MGCAMB, one can calculate an approximation to the derivatives dC_l/dp_i with respect to the N parameters p_i, namely

$$\frac{dC_l}{dp_i} \approx \frac{C_l(p_i + \delta p_i) - C_l(p_i - \delta p_i)}{2\delta p_i}. \tag{4.5}$$

In the limit that $\delta p_i \to 0$, (4.5) should become an equality. However, in practice this is not the case. As δp_i are shrunk, at some point they become small enough that numerical instability becomes

Amplitude	β_1	β_2	β_3	β_4	β_5	β_6	β_7	β_8	β_9	β_{10}	β_{11}
$\times 10^{-3}$	2	1	5	2	3	5	1	3	4	2	1

Table 4.1: Bin amplitudes used in testing the binning routine.

an issue. One obtains changes δC_l that are small and meaningless. But upon dividing by δp_i as in (4.5), one obtains a large number that is not a good approximation to the actual derivative. Of course, if the step size is too large, one cannot expect to get a good approximation to the derivative either. So one needs to find the sweet spot, where derivatives have began to converge, but the onset of numerical instabilities has yet to be reached. In practice, convergence is obtained when the step-sizes are smaller than but of the same order as the constraints obtained from the Fisher calculation.

4.4 Binning Routine

In order to study constraints on the functions $m(a)$ and $\beta(a)$ in more generality, we introduce a binning routine. It consists of smoothed step functions. We make use of a hyperbolic tangent function, letting $m(a)$, e.g., be defined as

$$m(a) = \sum_{i=1}^{N_{bin}-1} \frac{m_i - m_{i+1}}{2}[1 + tanh(\frac{a - a_{i+1}}{\Delta_i})], \tag{4.6}$$

where $\Delta_i \equiv \frac{a_{i+1}-a_i}{20}$ is the width of the i^{th} bin, m_i is the amplitude for the i^{th} bin, the a_i are the bin edges and $\beta(a)$ is similarly defined. The derivatives, calculated analytically, are also used in the code.

To illustrate the binning routine, $\beta(a)$ and $\dot{\beta}(a)$ are plotted in Figures 4.1 and 4.2. The amplitudes used for these plots are given in 4.1. These values are not typical of our actual runs, but rather chosen for illustrative and testing purposes only. The binning function (Equation 4.6) is seen to consist of smoothed step functions. As expected, the derivative is nonzero only near bin edges, where it is sharply peaked. It might be desirable to use an alternate binning routine in order to smooth the derivatives. However, it is known that this change does not significantly affect the results for similar models implemented in previous versions of MGCAMB.

Our code allows for $\beta(a)$ to be treated as a single constant or as a binned function. For forecasts we aim to use a large number of bins in order to perform PCA. Below we use 11 redshift bins for $m(a)$ and treat $\beta(a)$ as a constant β_0.

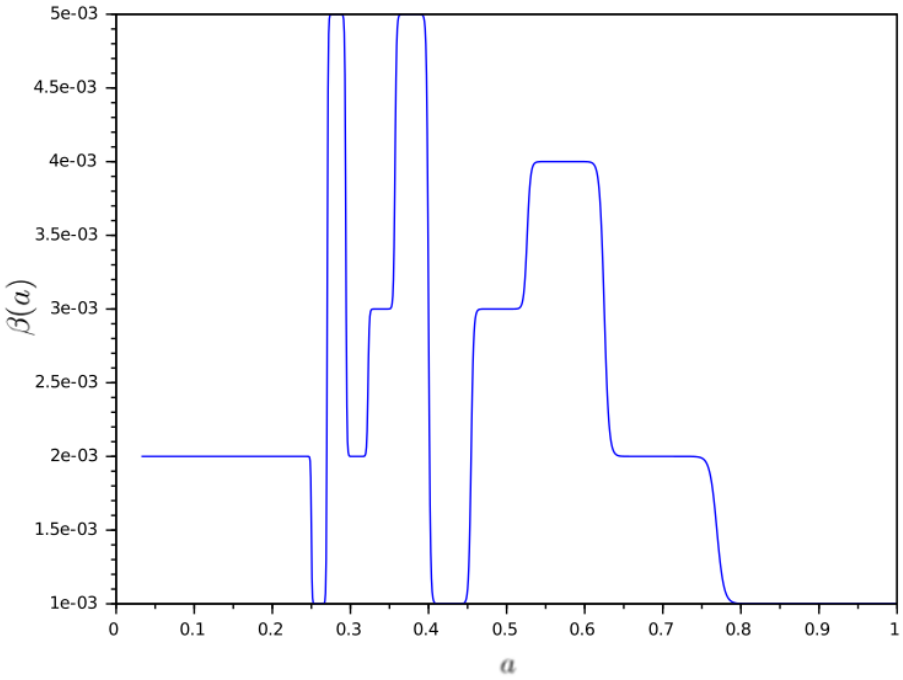

Figure 4.1: Binned $\beta(a)$.

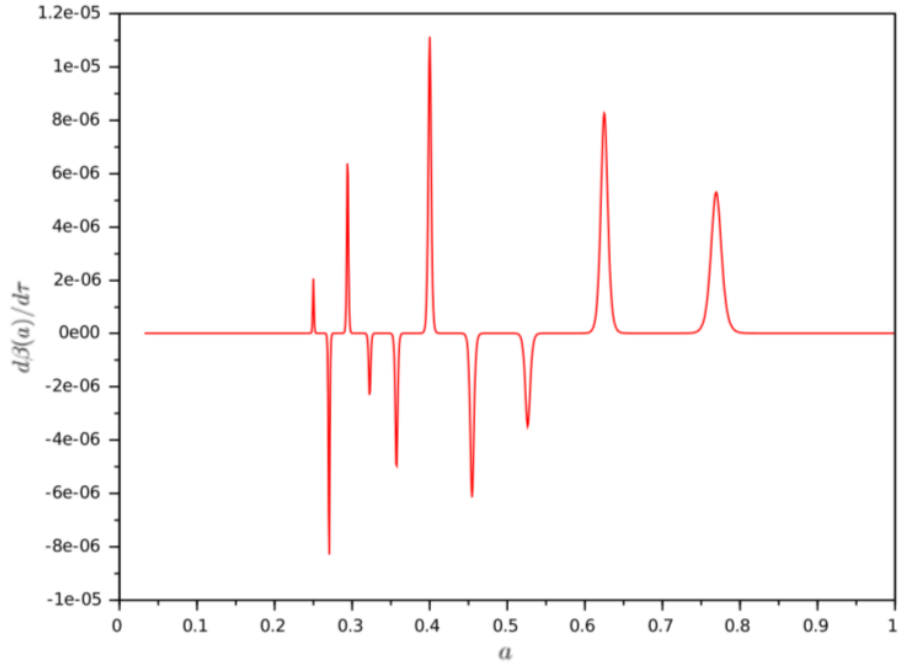

Figure 4.2: Binned $d\beta(a)/d\tau$.

Chapter 5

Results

5.1 Generalized Chameleon

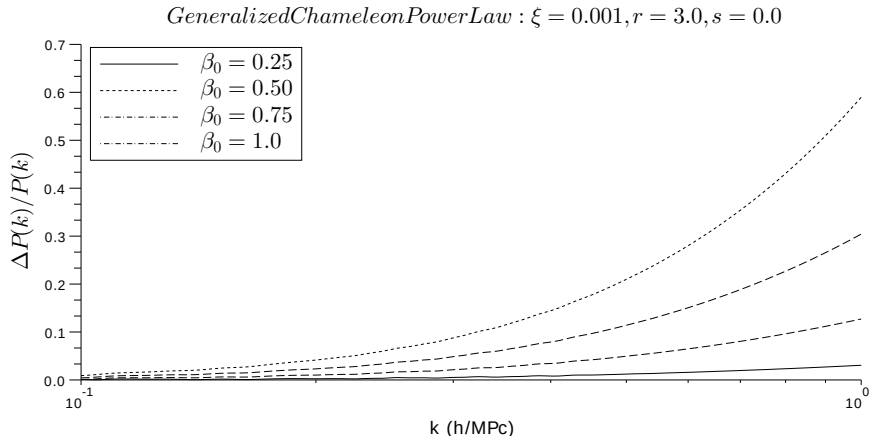

Figure 5.1: Relative difference in matter power spectrum for some Generalized Chameleon models compared to GR: varying β_0.

Figures 5.1-5.4 show the relative difference in the Matter Power Spectrum for some Generalized Chameleon models compared to GR. We note the trend general trend that the deviation from GR grows with k. This can be understood as follows. GR corresponds to $\gamma = \mu = 1$ in Equations (4.3) and (4.4). For $k << m$, $\gamma \to 1$ and $\mu \to 1$ in these equations. The parameter m is inversely related to the range of the new scalar force, while k is inversely related to the scale. When k is small relative to m, we are considering scales much larger than the range of the force, and the modifications to GR are negligible. As k grows, we begin to consider scales on which the new force becomes important.

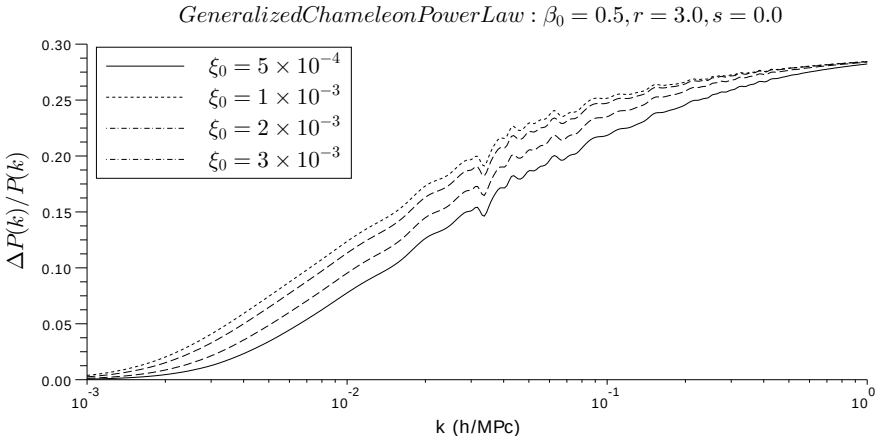

Figure 5.2: Relative difference in matter power spectrum for some Generalized Chameleon models compared to GR: varying ξ.

Parameter	$\omega_b h^2$	$\omega_c h^2$	H_0	τ	$\sum m_\nu$	w	$\ln(10^{10} A_s^2)$	n_s
Gen Cham I	0.0226	0.112	70	0.09	0	-1	3	0.96

Table 5.1: Fiducial values used for standard cosmological parameters.

Figures (5.5-5.7) show the relative difference in the CMB temperature power spectrum for extreme Generalized Chameleon models. We also note that numerical issues arise before an appreciable difference in the CMB due to extreme β_0 is seen, hence the absence of a fourth figure. Comparing the CMB plots to those for matter power spectrum suggests that these modified gravity parameters are best constrained by LSS observables, which are related to the growth of perturbations.

Table 5.1 lists the fiducial values used for the standard cosmological parameters in our forecasts. Table 5.2 lists the fiducial values used in our Fisher forecasts for Generalized Chameleon models. Here $h \equiv H_0/100$. The relative deviation from GR in the Matter power spectrum is plotted in Figure 5.8. The parameter constraints $\sqrt{F^{-1}{}_{ii}}$ (where i labels the parameters), resulting from the Fisher forecast, are collected in Table 5.3. The 1σ confidence interval for xi obtained by [16] using current data is $[10^{-6.1}, 10^{-1.5}]$. From Table 5.2 we see that LSST can be expected to improve this to at least $\xi_0 < 10^{-3}$. We do not obtain a lower bound for ξ_0, since $\xi > 0$ strictly while our constraint σ_{ξ_0} is of

Parameter	β_0	r	ξ_0	s
Gen Cham I	0.41	3	9.0e-4	0

Table 5.2: Fiducial values used for the Generalized Chameleon forecast.

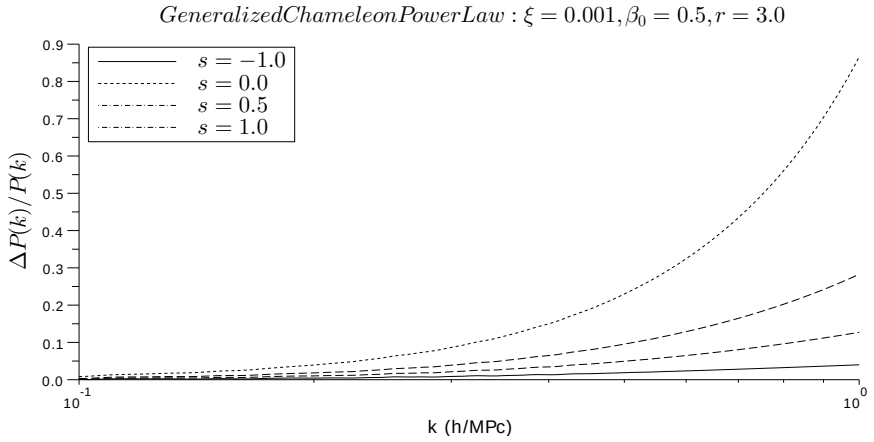

Figure 5.3: Relative difference in matter power spectrum for some Generalized Chameleon models compared to GR: varying s.

Parameter, p	$\omega_b h^2$	$\omega_c h^2$	H_0	τ	w	n_s	β_0	r	ξ_0
σ_p	6.7e-5	2.3e-4	0.21	1.1e-3	6.8e-3	2.5e-3	0.25	1.0	1.1e-3

Table 5.3: Standard deviations forecast for Generalized Chameleon and cosmological parameters.

the same order as our fiducial value for ξ_0.

In Figures 5.9-5.14 we plot the 1σ contour plots. For each combination of Generalized Chameleon model parameters or w, we have plotted contours corresponding to $WL + CMB$, $GC + CMB$, $WL+GC$, and $WL+GC+CMB$, where $WL+CMB$, e.g., refers to including all auto-correlations and cross-correlations of the N_{WL} weak lensing bins and CMB T/E that are provided by MGCAMB.

It is clear in all cases that CMB offers very weak constraints. This is evident from that the contours for $WL + GC$ are almost identical to those for $WL + GC + CMB$. The model parameters are best constrained by WL and GC. In general, we see stronger constraints from WL than GC (both considered in combination with CMB). Beyond this, the cross-correlations WL X GC, included in the WL + GC curves, improve the constraints significantly.

ξ_0 and r are highly degenerate, no matter which observables are considered. This is to be expected as both appear in the same function (see Equation 2.27)

$$m(a) = \frac{H_0 a^{-r}}{\xi_0}. \tag{5.1}$$

w is degenerate with r and also ξ_0 when considering WL or GC separately, but including their cross-correlations helps to break these degeneracies. Meanwhile, w is not strongly degenerate with β_0. β_0 and r are highly degenerate, and no combination of observables considered breaks this degeneracy. We can increase the coupling of the field to matter provided that we simultaneously

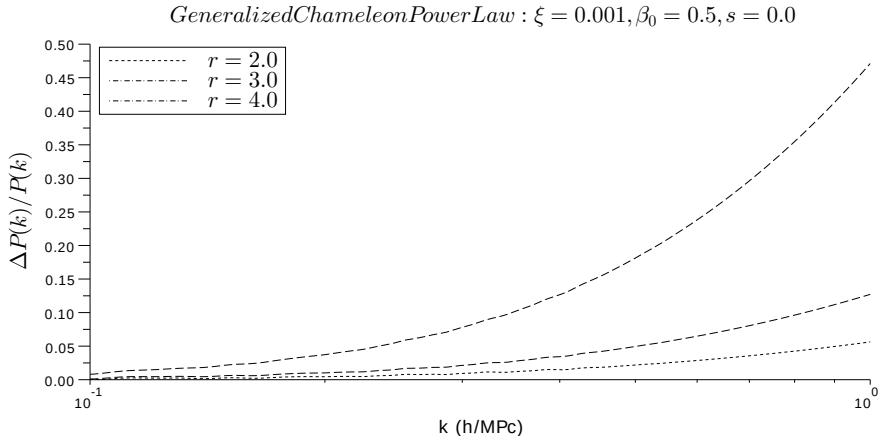

Figure 5.4: Relative difference in matter power spectrum for some Generalized Chameleon models compared to GR: varying r.

Parameter	β_0	$\xi_i = H_0/m_i$
Binned Model I	0.1	1.0e-3

Table 5.4: Fiducial values used for the Binned Model I forecast.

increase r, how quickly the range decays. On the other hand, while β_0 is degenerate with ξ_0 considering $CMB + GC$ only, one need only consider WL to break this degeneracy.

5.2 Binned $\{\xi(a)\}$

For the binned models, we assume $\beta(a) \equiv \beta_0 = constant$, and bin $\xi(a)$ into 11 redshift bins. As a fiducial, we take $\xi(a)$ flat, i.e. all of the amplitudes ξ_i are equal. Hence the fiducial models are equivalent to a Generalized Chameleon model with $r = s = 0$. For illustration purposes, we have produced plots of the relative difference in the matter power spectrum compared to GR for various choices of β_0 and ξ_0 for $r = s = 0$. These appear in Figures. The fiducials we use here are presented in Table 5.4.

PCA was performed on the resulting Fisher matrix- i.e. F^{-1} was diagonalized. The errors of the PC's are given in Figure 5.17. The eigenvalues for the first 5 PC's are plotted in Figure 5.18.

We note that the first PC rises at $a \approx 0.3$ and is flat afterwards. Hence $m(a)$ is sensitive to these observables at $a > 0.3$. Of the rest, only PC 5 shows a long coherent structure. From Figure 5.17 we can see that the first PC is signifcantly better constrained than subsequent PC's. Hence this is expected to be representative of noise rather than something physical.

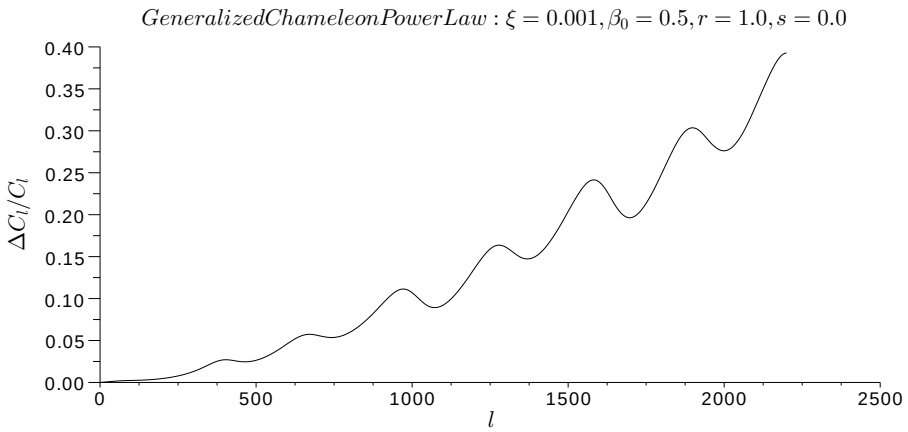

Figure 5.5: Relative difference in CMB power spectrum for a Generalized Chameleon model compared to GR: extreme r.

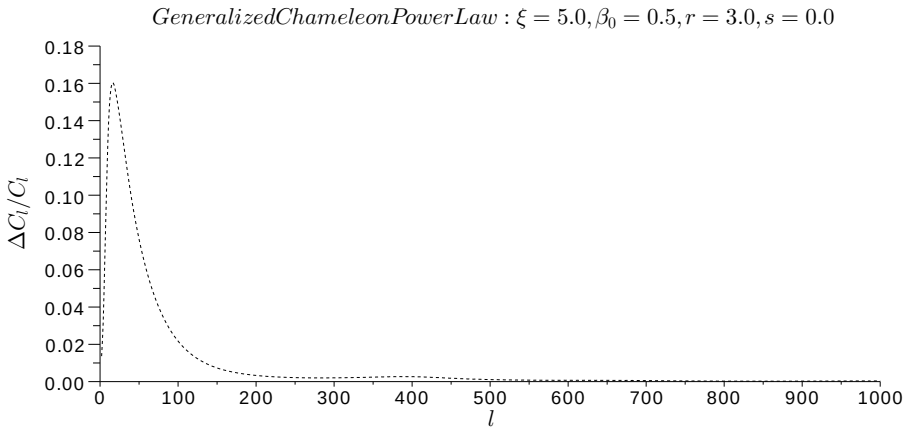

Figure 5.6: Relative difference in CMB power spectrum for a Generalized Chameleon model compared to GR: extreme ξ.

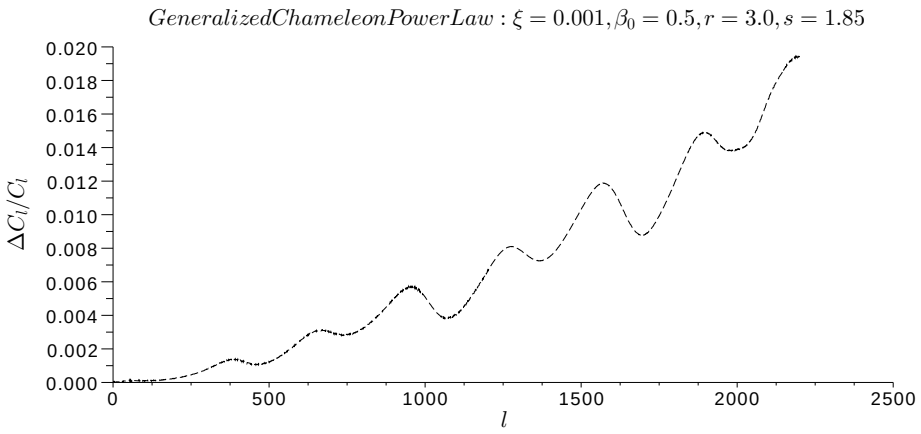

Figure 5.7: Relative difference in CMB power spectrum for a Generalized Chameleon model compared to GR: extreme s.

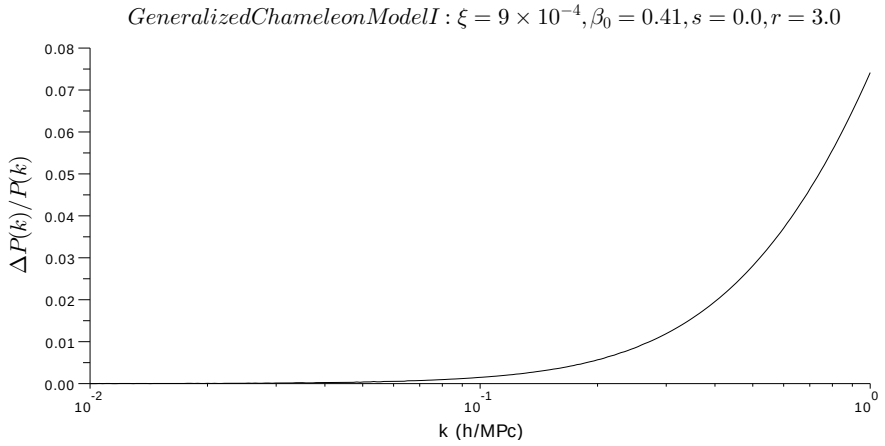

Figure 5.8: Relative difference in matter power spectrum for Generalized Chameleon model I compared to GR.

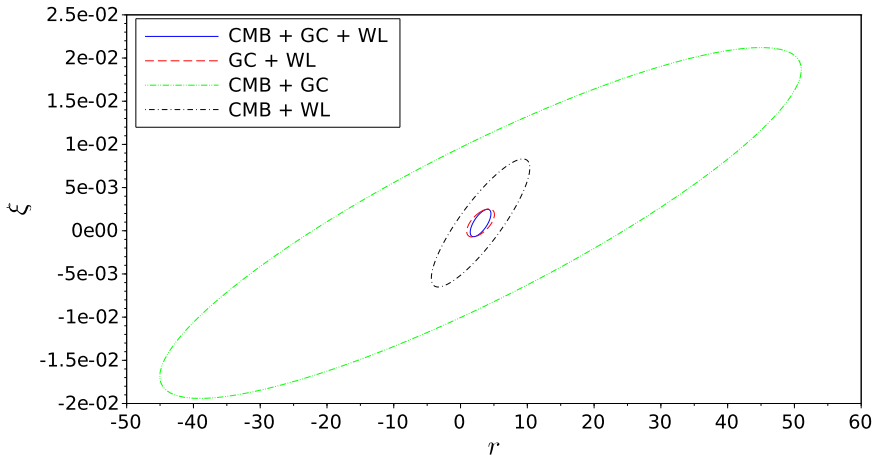

Figure 5.9: ξ_0-r 1σ contour for Generalized Chameleon I model parameters.

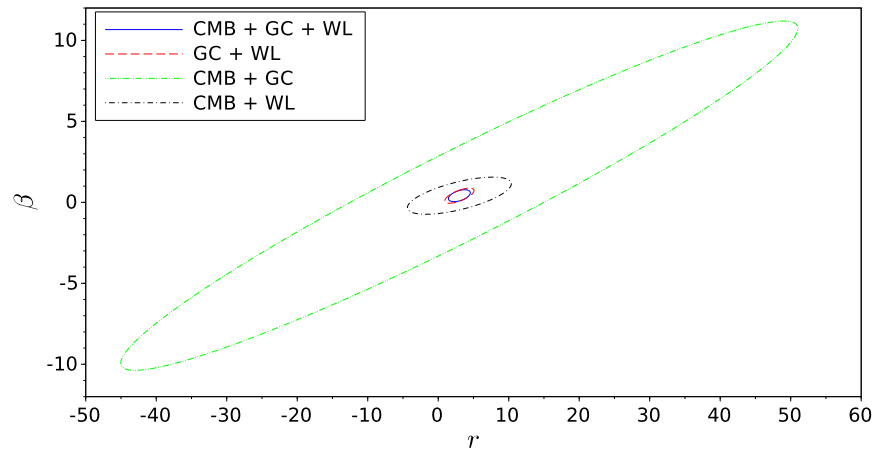

Figure 5.10: β-r 1σ contour for Generalized Chameleon I model parameters.

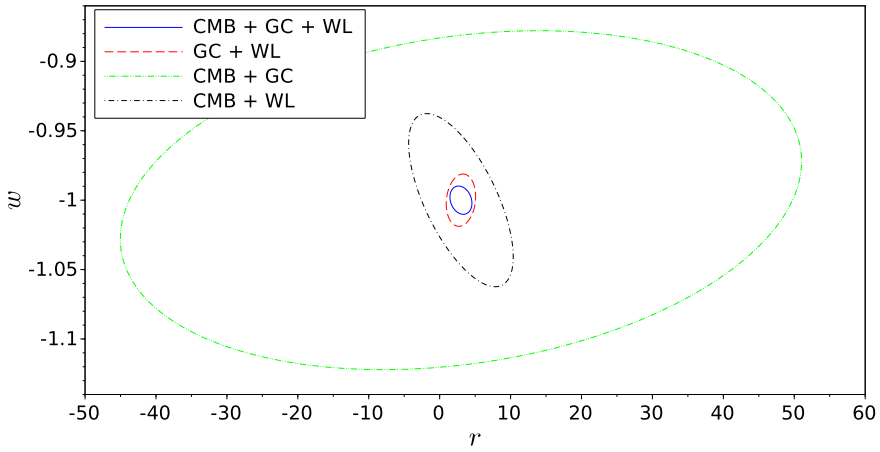

Figure 5.11: w-r 1σ contour for Generalized Chameleon I model parameters.

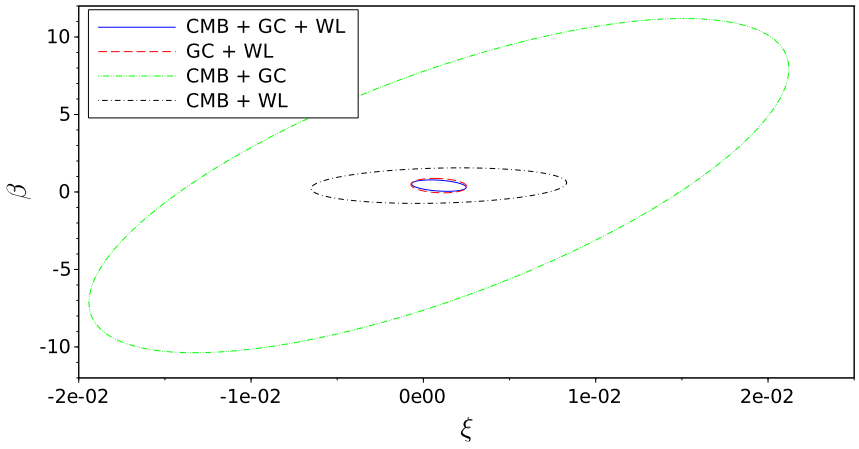

Figure 5.12: β_0-ξ_0 1σ contour for Generalized Chameleon I model parameters.

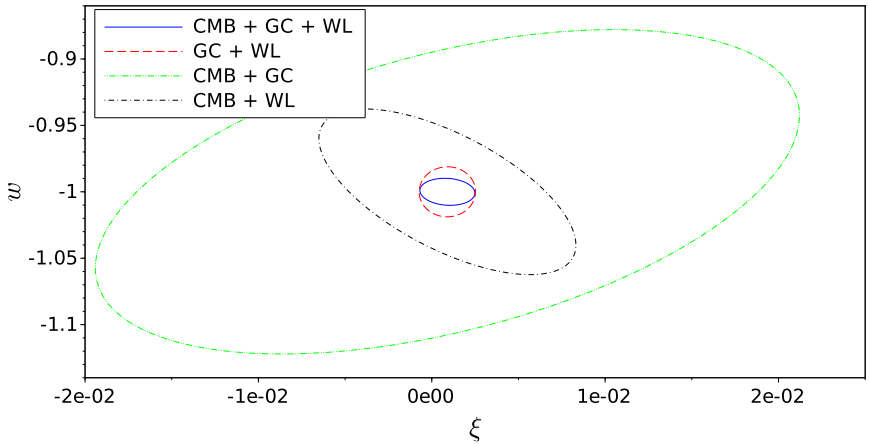

Figure 5.13: w-ξ_0 1σ contour for Generalized Chameleon I model parameters.

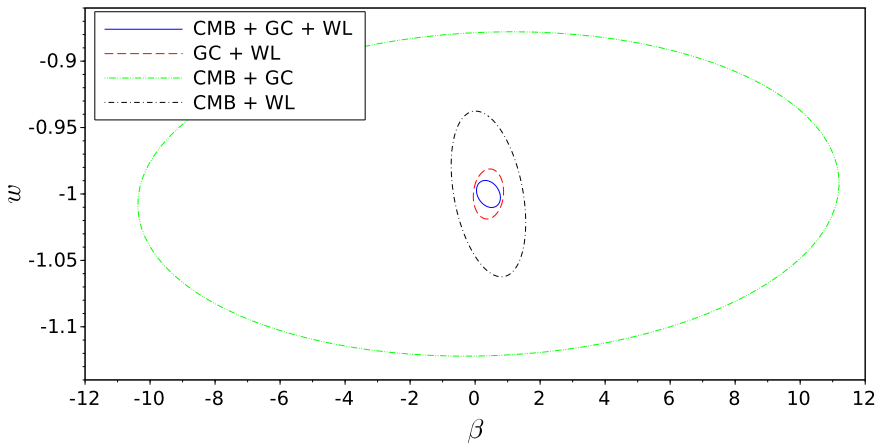

Figure 5.14: w-β_0 1σ contour for Generalized Chameleon I model parameters.

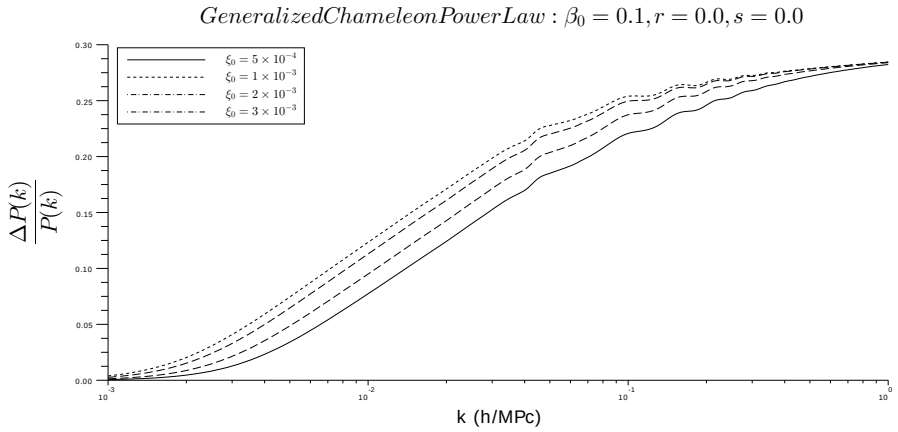

Figure 5.15: Relative difference in matter power spectrum as compared to GR for some Generalized Chameleon models with $r = s = 0$: varying ξ_0.

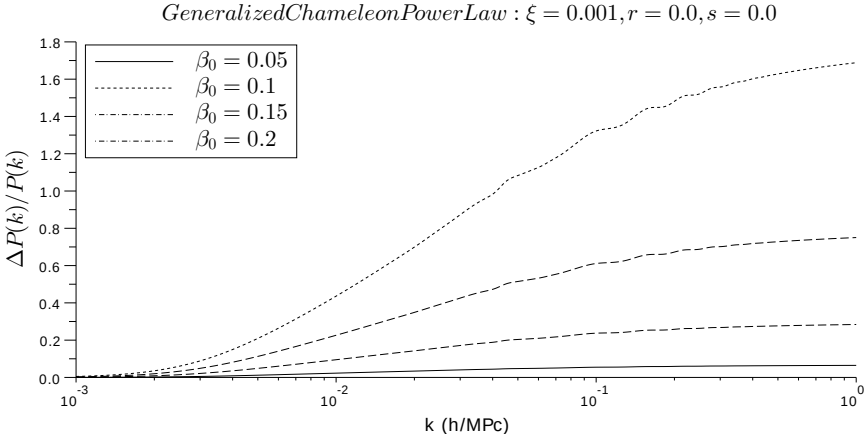

Figure 5.16: Relative difference in matter power spectrum as compared to GR for some Generalized Chameleon models with $r = s = 0$: varying β_0.

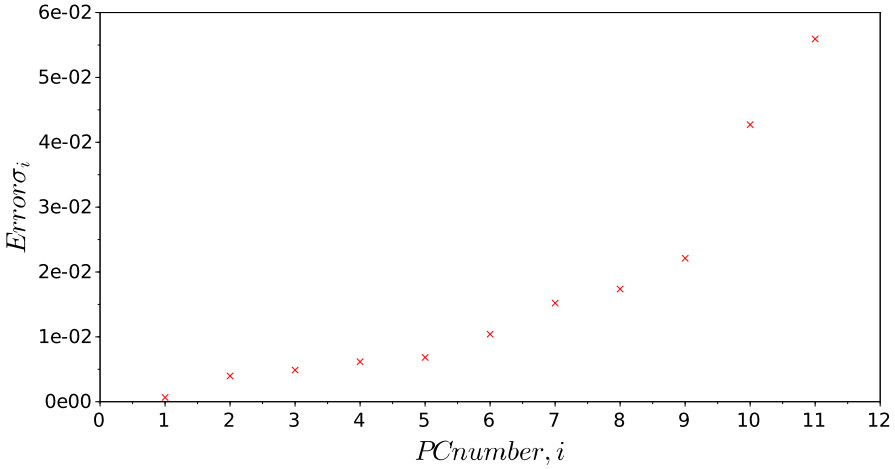

Figure 5.17: Normalized errors σ_i of the first 5 PC's for Binned Model I,after marginalizing over all parameters except β_0 and $m(a)$.

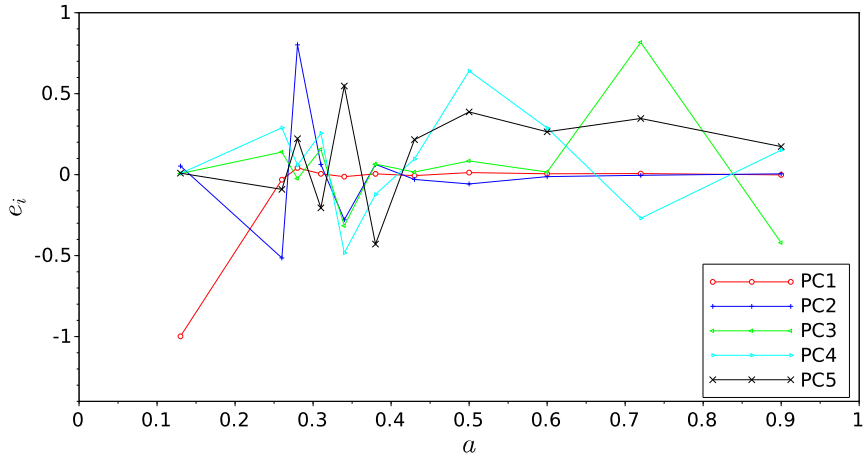

Figure 5.18: Normalized eigenvectors of the Fisher Matrix F for Binned Model I, after marginalizing over all parameters except β_0 and $m(a)$.

Chapter 6

Conclusion

In this thesis, we have introduced our implementation of the $\{m(a), \beta a\}$ parametrization of STT in MGCAMB, and presented Fisher Forecasts for a few popular Screened Modified Gravity models. Forecasts for the additional models discussed in Chapter 2 are in progress. As with the Chameleon Model, generalizations of the Symmetron and Dilaton models exist, and can be readily implemented within our code. It might also be of interest to bin $\beta(a)$ in addition to $m(a)$, and to use a larger number of bins. There is an alternate set of expression for $\mu(k, a)$ and $\gamma(k, a)$ [12]. Namely,

$$\gamma(k, a) = \frac{1 - \epsilon(k, a)}{1 + \epsilon(k, a)} \tag{6.1}$$

$$\mu(k, a) = 1 + \epsilon(k, a), \tag{6.2}$$

where

$$\epsilon(k, a) \equiv \frac{2\beta(k, a)^2}{1 + m(k, a)^2 a^2/k^2}. \tag{6.3}$$

One could introduce this parametrization into our code, effectively replacing two functions of a alone with one function of k and a, proceeding to perform PCA on this 2-D function. We note that our binning routine is already capable of binning in k as well as a.

We have found that the models we have studied are constrained primarily by LSS. Meanwhile, the constraints from the CMB are quite weak. One possible generalization would be to allow for distinct couplings β_i of the field to each matter species i. Allowing for distinct coupling to CDM and baryonic matter was shown to lead to non-trivial constraints on $m(a)$ from the CMB in [32]. There it was also suggested that the CMB and LSS are complementary in that they constrain distinct features of $m(a)$.

Bibliography

[1] S.S. Shapiro, J.L. Davis,D.E. Lebach and J.S. Gregory, Phys. Rev. D **92**(12): 121101 (2004)

[2] B. Bertotti, Nature **D425**(6956):37 (2003).

[3] C.G. Clifton, P.G. Ferreira, A. Padilla and C. Skordis, Phys. Rep. **513**:1-189 (2012). [arXiv:1106.2476v3[astro-ph.CO]]

[4] G. A. Krasinskii, E. V. Pit'eva, M. L. Sveshnikov and L. I. Chuniaeva, Celest. Mech. Dyn. Astron. **55**:1-23 (1993).

[5] S. M. Carroll, *Spacetime and Geometry: An Introduction to General Relativity*(Adison-Wesley, San Francisco, 2004).

[6] C. W. Misner, K. S. Thorne and J. A. Wheeler, *Gravitation*(W.H. Freeman and Company, New York, 1973).

[7] R. Durrer, *The Cosmic Microwave Background*(Cambridge, New York, 2008).

[8] C. Pryke, N. W. Halverson, E. M. Leitch, J. Kovac and J. E. Carlstrom, Astrophys. J. **568**:46-51 (2002).

[9] S. Dodelson, *Modern Cosmology*(Academic Press, New York, 2003).

[10] C. -P. Ma and E. Bertschinger, Astrophys. J. **455**:7-25 (1995) [arXiv:9506072[astro-ph]].

[11] J. F. Navarro, C. S. Frenk, and S. D. White, Astrophys. J. **462**:563-575 (1996) [arXiv:9508025 [astro-ph]].

[12] P. Brax, A. -C. Davis, B. Li and H. A. Winther, Phys. Rev. D **86**, 044015 (2012) [arXiv:1203.4812 [astro-ph.CO]].

[13] P. Brax, A. -C. Davis and B. Li, Phys. Lett. B **715**, 38 (2012) [arXiv:1111.6613 [astro-ph.CO]].

[14] L. Pogosian, A. Silvestri, K. Koyama and G. -B. Zhao, Phys. Rev. D **81**, 104023 (2010) [arXiv:1002.2382v2 [astro-ph]].

[15] G.-B. Zhao, L. Pogosian, A. Silvestri and J. Zylberberg, Phys. Rev. D **79**, 083513 (2009) [arXiv:0809.3791v2 [astro-ph]].

[16] A. Hojjati, A. Plahn, L. Pogosian, P. Brax and A. -C. Davis, In Progress.

[17] http:/cosmologist.info/cosmomc

[18] J. Khoury and A. Weltman, Phys. Rev. D **69**, 044026 (2004) [arXiv:0309411v2 [astro-ph]].

[19] T.P. Waterhouse, arXiv:0611816[astro-ph].

[20] W. Hu and I. Sawicki, Phys. Rev. D **76**, 064004 (2007) [arXiv:0705.1158 [astro-ph]].

[21] K. Hinterbichler and J. Khoury, Phys. Rev. Lett. **104**, 231301 (2010) [arXiv:1001.4524 [hep-th]].

[22] P. Brax, C. van de Bruck, A. -C. Davis and D. Shaw, Phys. Rev. D **82**, 063519 (2010) [arXiv:1005.3735 [astro-ph]].

[23] (REF TEGMARK et al arXiv:astro-ph/9603021) Astrophys. J. **480**:25-35 (1997) [arXiv:9603021v2 [astro-ph]].

[24] http://www.lsst.org

[25] Z. Ivezic *et al.*, arXiv:0805.2366v4[astro-ph].

[26] http://sci.esa.int/planck

[27] [Planck Collaboration], [arXiv:0604069[astro-ph]].

[28] D. Huterer and G. Starkman. Phys. Rev. Lett. **90**, 031301 (2003).

[29] http://www.camb.org.

[30] http://www.sfu.ca/gza5/MGCAMB.html

[31] http://www.sfu.ca/ aha25/MGCAMB.html

[32] P. Brax and A. -C. Davis, Phys. Rev. D **85**, 023513 (2011) [arXiv:1109.5862v2 [astro-ph]].